

ABSTRACT

Investigation of Cruzain Inhibition by Thiosemicarbazone Compounds

Isaac Lill

Director: Mary Lynn Trawick, Ph.D.

Chagas disease, the result of infection by the protozoan parasite *Trypanosoma cruzi*, is transmitted by blood-feeding insect vectors that are members of the Reduviidae family called kissing bugs. The vectors are found throughout Latin America, and predominantly in Texas, New Mexico, and Arizona in the United States. Chagas is responsible for about 12,000 deaths per year and it is estimated that 6-8 million people worldwide are infected. There is currently no approved treatment for eliminating the parasite during its chronic phase after it has migrated into tissue. Thus, there is an unmet need for treatment agents. One validated target is cruzipain, a potent cysteine protease that is necessary for the parasite's survival throughout its life cycle including immune evasion, tissue infection, processing and degradation of proteins, and reproduction. This study used cruzain, which is a recombinant form of cruzipain, to test inhibition of enzyme activity with a focused library of thiosemicarbazone compounds. Potential inhibitors were evaluated using a fluorogenic enzyme assay to assess the cleavage of 7-amino-4-methylcoumarin (AMC) from the cruzain substrate Z-Phe-Arg-AMC. Several compounds in this series had IC₅₀ values less than 100 nM with the substituted benzophenone thiosemicarbazone KGP434 being the most effective (IC₅₀ = 17 nM). Kinetics studies were performed to determine the mode of inhibition. Progress curves and reversibility studies indicated that KGP434 is an active site directed, time-dependent, and slowly reversible inhibitor of cruzain. Docking studies showed the positioning of the aryl groups in the hydrophobic S2 and S3 pockets places the thiosemicarbazone moiety in close proximity to cysteine-25 which provides evidence for covalent inhibition.

APPROVED BY DIRECTOR OF HONORS THESIS

Dr. Mary Lynn Trawick,
Department of Chemistry and Biochemistry

APPROVED BY THE HONORS PROGRAM

Dr. Elizabeth Corey, Director

DATE: _____

INVESTIGATION OF CRUZAIN INHIBITION BY THIOSEMICARBAZONE
COMPOUNDS

A Thesis Submitted to the Faculty of
Baylor University
In Partial Fulfillment of the Requirements for the
Honors Program

By
Isaac D. Lill

Waco, TX

May 2018

TABLE OF CONTENTS

TABLE OF CONTENTS.....	ii
LIST OF FIGURES	iv
LIST OF TABLES.....	iii
LIST OF ABBREVIATIONS.....	iv
CHAPTER ONE: INTRODUCTION.....	1
<i>Trypanosoma cruzi</i> Life Cycle and Transmission.....	1
<i>Vector Characteristics and Distribution in the US</i>	3
<i>Disease Characteristics</i>	5
<i>Current Treatment Methods</i>	5
<i>Chagas in the United States</i>	6
<i>Cruzipain</i>	10
<i>Catalytic Mechanism of Cruzain</i>	13
CHAPTER TWO: MATERIALS AND METHODS	15
<i>Materials and Instrumentation</i>	15
<i>Preparation of Stock Solutions</i>	16
<i>Preparation of Assay Solutions and Final Assay Conditions</i>	17
<i>Experimental Methods</i>	20
<i>Obtaining an AMC Standard Curve</i>	20

<i>Determination of K_M, k_{Cat}, and V_{max}</i>	20
<i>Determination of Inhibition by Thiosemicarbazones at 10 μM</i>	21
<i>Measurement of IC_{50} Values</i>	21
<i>Determination of Time-Dependence of KGP434</i>	22
<i>Determination of the Mode of Inhibition by KGP434</i>	22
<i>Determination of Reversibility for KGP434</i>	23
CHAPTER THREE: RESULTS AND DISCUSSION.....	24
<i>AMC Standard Curve</i>	24
<i>Cruzain – Z-FR-AMC Kinetics</i>	25
<i>Work Flow for Inhibitor Screening and Characterization</i>	27
<i>High Concentration Screening of Inhibitors and Determination of IC_{50} Values</i>	27
<i>Advanced Kinetic Studies of KGP434</i>	32
<i>Molecular Modeling</i>	35
<i>Proposed Mechanism of Inhibition</i>	37
<i>Conclusions</i>	38
APPENDIX A.....	40
APPENDIX B.....	47
REFERENCES	52

LIST OF FIGURES

Figure 1: Trypomastigotes in blood taken from a canine in Texas (left), amastigotes in canine cardiac tissue taken from a canine in also in Texas (right)	1
Figure 2: <i>Trypanosoma cruzi</i> life cycle.....	3
Figure 3: Examples of the 10 species of kissing bugs found in the US (one additional species is found very rarely)	4
Figure 4: Distribution of triatomine species in the US.	4
Figure 5: Distribution of estimated cases of Chagas disease by state.....	7
Figure 6: Distribution of confirmed canine infections in Texas.	9
Figure 7: Amino acid sequence of mature cruzain (PDB: 1ME3).....	12
Figure 8: Amino acid sequence of preprocruzain. Legend: Green: Signal Peptide; Blue: Propeptide; Red: Mature Cruzain; Purple: C-Terminal.	13
Figure 9: Layout of the 96-well plates used in the kinetic assays.	15
Figure 10: Z-FR-AMC cleavage by cruzain	24
Figure 11: Standard curve of fluorescence versus AMC concentration.	25
Figure 12: Fluorescence versus time for multiple reactions with varying concentrations of substrate.	26
Figure 13: Michaelis-Menten curve of cruzain with Z-FR-AMC substrate.	26
Figure 14: Workflow for inhibitor screening a characterization	27
Figure 15: Fractional activity plotted against the log of the inhibitor concentration allows for determination of the IC ₅₀	28

Figure 16: Progress curve of cruzain in the presence of increasing concentrations of KGP434, demonstrating a time-dependent mode of inhibition.	33
Figure 17: Increasing inhibition of cruzain was observed with decreasing substrate concentrations in the presence of KGP434 (1 μ M).	34
Figure 18: k_{obs} vs. substrate concentration. The shape of the plot indicates that both inhibitor (KGP434) and substrate compete for the same site.	34
Figure 19: Reversibility study of KGP434	35
Figure 20: Molecular model of KGP434 bound to cruzain (PDB:1ME3).....	36
Figure 21: Proposed mechanism for the covalent inhibition of cruzain by KGP434	37
Figure 22: IC ₅₀ results for KGP 68	40
Figure 23: IC ₅₀ results for KGP 382	41
Figure 24: IC ₅₀ results for KGP 384	41
Figure 25: IC ₅₀ results for KGP 385	42
Figure 26: IC ₅₀ results for KGP 388	42
Figure 27: IC ₅₀ results for KGP 402	43
Figure 28: IC ₅₀ results for KGP 406	43
Figure 29: IC ₅₀ results for KGP 421	44
Figure 30: IC ₅₀ results for KGP 434	44
Figure 31: IC ₅₀ results for KGP 434 using 5 μ M substrate	45
Figure 32: IC ₅₀ results for KGP 435	45
Figure 33: IC ₅₀ results for KGP 451	46

LIST OF TABLES

Table 1: Estimated number of Chagas cases and number of cases confirmed by blood screening by state.....	7
Table 2: Amino acid composition of mature cruzain.....	12
Table 3: Preparation of inhibitor stocks A-F	17
Table 4: Assay Buffer Preparation.....	18
Table 5: Enzyme buffer preparation	18
Table 6: Preparation of inhibitor solutions. The final [I] indicates the concentration of inhibitor on the reaction solution	19
Table 7: Preparation of substrate solutions. Final [S] indicates the concentration of substrate in the reaction solution.....	19
Table 8: Dilution buffer components.....	23
Table 9: Compound structure and IC ₅₀ values.....	29

LIST OF ABBREVIATIONS

Cys	Cysteine
DMSO	Dimethylsulfoxide
DTT	Dithiothreitol
E	Enzyme
EDTA	Ethylenediaminetetraacetic Acid
F	Phenylalanine
His	Histidine
I	Inhibitor
IC ₅₀	Inhibitor concentration required to reduce enzyme activity by 50%
k_{cat}	Enzyme Turnover Number
kDa	Kilodalton
K_M	Michaelis-Menten Constant
k_{obs}	Rate Constant for Conversion of v_o to v_s
mM	Millimolar
NaOAc	Sodium Acetate Buffer
nM	Nanomolar

R	Arginine
S	Substrate
<i>T. cruzi</i>	<i>Trypanosoma cruzi</i>
V_{\max}	Maximal Velocity
v_o	Initial velocity
v_s	Steady-State Velocity
Z-FR-AMC	7-Amino-4-methylcoumarin, N-CBZ-L-phenylalanyl-L-arginine amide, hydrochloride
μM	Micromolar

CHAPTER ONE

Introduction

Chagas disease, the result of infection by the protozoan parasite *Trypanosoma cruzi*, is transmitted by blood-feeding insect vectors that are members of the Triatominae sub-family of the Reduviidae family which are also called kissing bugs.¹ The vectors are common in Latin America where the disease is endemic but can also be found in the United States predominately in Texas, New Mexico, Arizona, and Florida.² There are an estimated 6-8 million infected people worldwide, and the disease is responsible for approximately 12,000 deaths every year.³ Additionally, Chagas diseases results in 97,500 YLDs (years lived with disabilities) every year due to its significant morbidity.⁴ As a result, it is the highest contributor of DALYs (disability adjusted life years) of all parasitic diseases in Central America.⁵

Trypanosoma cruzi Life Cycle and Transmission

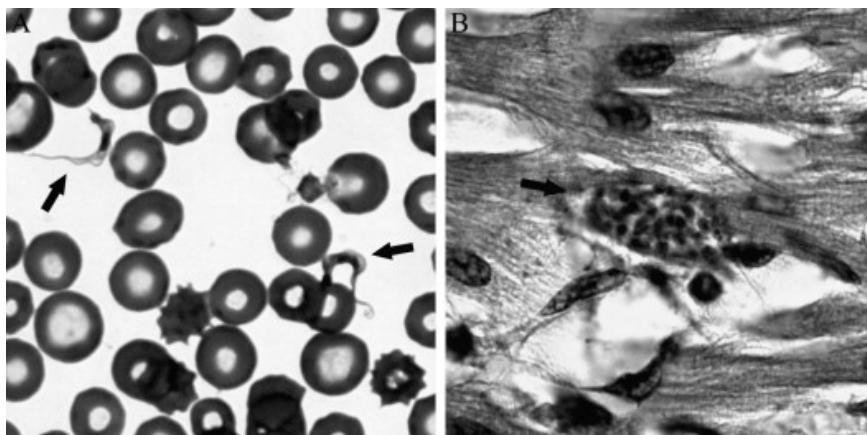


Figure 1: Trypomastigotes in blood taken from a canine in Texas (left), amastigotes in canine cardiac tissue taken from a canine in Texas (right).⁶

T. cruzi, a protozoan parasite, goes through a complicated life cycle in the triatomine insect vector and in mammalian hosts. After taking a blood meal from a mammal, the infected triatomine defecates, and the feces contains *T. cruzi* in its non-replicative, flagellated trypomastigote phase. These trypomastigotes invade cells in the human body where they transform into replicative un-flagellated amastigotes which undergo binary fission. Amastigotes then transform into trypomastigotes which enter the blood stream. These trypomastigotes can enter other host cells and repeat the cycle, or they may be ingested by another triatomine insect that feeds on the mammalian host. If this occurs, the trypomastigotes transform into epimastigotes in the insect's midgut where they replicate. The epimastigotes transform back into non-replicative trypomastigotes in the insect's hindgut and are deposited in feces at the site of the insect's next blood meal. This life cycle is illustrated in Figure 1. The insect vectors do not appear to be harmed by infection with *T. cruzi*.⁷⁻⁹

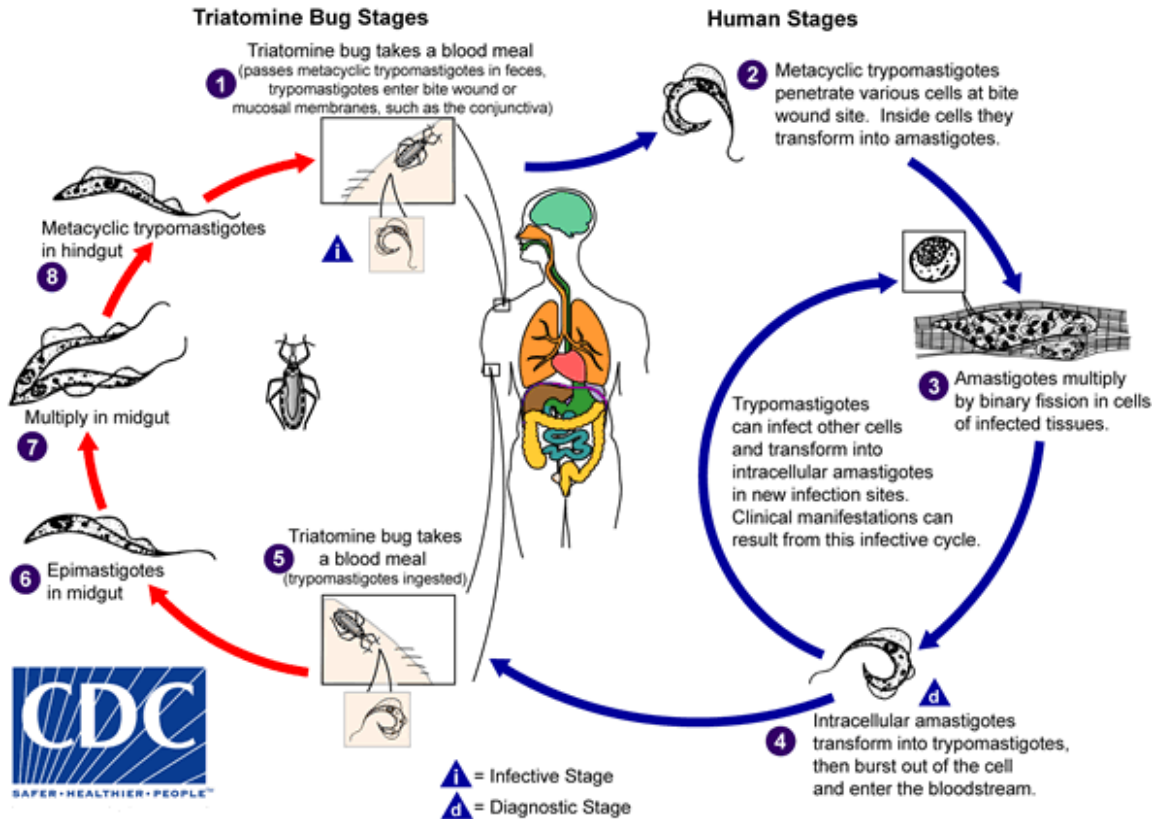


Figure 2: *Trypanosoma Cruzi* life cycle¹⁰

Vector Characteristics and Distribution in the US

T. cruzi is spread by infected insects of the family Revudiiidae and the genus *Triatoma*. These bugs, also known as “kissing bugs” typically inhabit the burrows of mammals or the human habitats and peridomestic structures. These insects ingest blood from mammals to which they live in close proximity.¹¹ Approximately 100 species of triatomine insects are present throughout the Americas, and one species, *Triatoma rubrofasciata*, has been spread to a variety of cities around the world.¹² Kissing bugs are recognizable by their long, thin head. Several examples are shown in Figure 3.

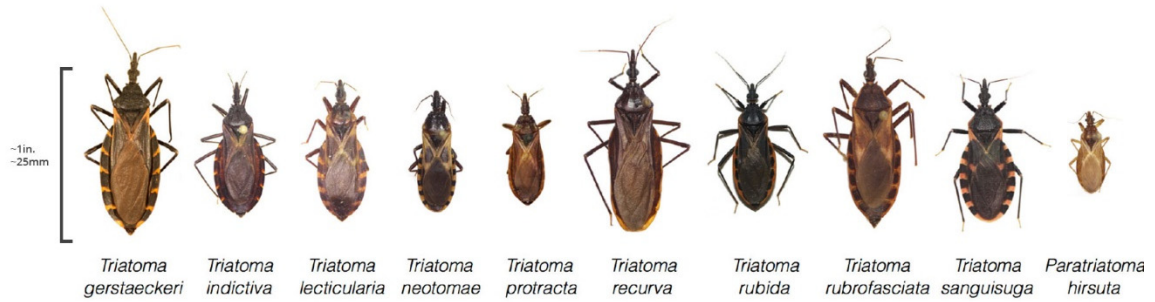


Figure 3: Examples of the 10 species of kissing bugs found in the US (one additional species is found very rarely).¹³

Ten species of kissing bugs are commonly found in the US. The most widespread is *T. sanguisuga*, and 50-60% of the species is infected with *T. cruzi*.^{14,15} In Texas, *T. gerstaeckeri*, is the most prevalent and has an infection rate around 63%.² Both the prevalence and high infection rate of these insects contribute to the risk of infection in the southern regions of the US.

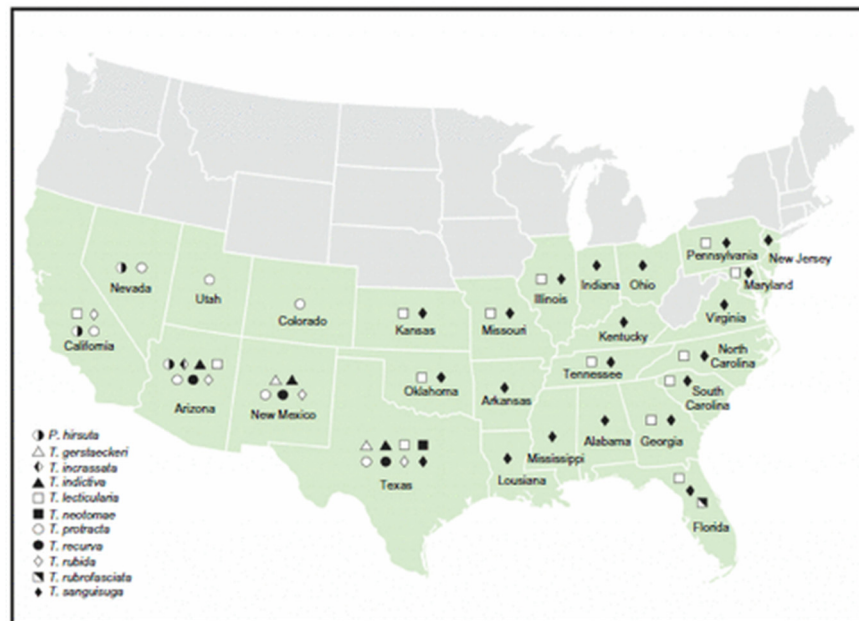


Figure 4: Distribution of triatomine species in the US.¹²

Disease Characteristics

After contact with *T. cruzi*, the disease begins the acute phase. At this point, there is detectable parasitemia but often only mild symptoms or no symptoms at all. After four to eight weeks the acute phase ends, and the indeterminate chronic phase begins. In this stage, the parasite concentration in tissues decreases significantly, and any symptoms are spontaneously resolved. However, the parasite is not eliminated entirely and remains present in certain tissues indefinitely.⁷ About 30-40% of infected people progress from the indeterminate chronic phase to the determinate chronic phase with the development of symptoms. These symptoms include cardiovascular disease and gastrointestinal disorders like megacolon and megaesophagus.^{16,17} The majority of Chagas related morbidity and mortality results from arrhythmias, aneurysms, and heart failure. Moreover, Chagas-induced cardiomyopathies tend to be less responsive to treatment than cardiomyopathies with other etiologies.^{16,18}

Current Treatment Methods

Despite the severity and prevalence of Chagas disease, few advancements in its treatment have been made in the past several decades, and treatment options remain extremely limited. Currently, the only available options are benznidazole and nifurtimox. These drugs are highly effective during the acute phase, but, are not generally curative during the chronic phase.¹⁹ Since the acute phase is often asymptomatic, treatment is often not initiated until the chronic phase. At this stage, benznidazole has been shown to decrease the parasite load which could impede the progression of cardiovascular or gastrointestinal pathologies.⁷ However, recent research has indicated that chronic-phase treatment with benznidazole does not appear to affect the outcomes of Chagas related

cardiac disease.²⁰ Moreover, both drugs have significant side effects which significantly decrease their utility in treating Chagas disease. Benznidazole is considered the safer drug between the two, but 85% of patients experience adverse side-effects and 20% are unable to complete the treatment due to these side-effects.²¹ The FDA recently approved benznidazole for Chagas treatment, but only for children 2-12 years of age who generally tolerate the drug better than adults.^{19,22}

Chagas in the United States

Chagas disease has historically received little attention in the United States. However, the influx of immigration from Latin America over the past several decades has resulted in a growing number of Chagas cases in the US. Estimates based on the prevalence of Chagas disease in the origin countries of Latin American immigrants places the number of infected individuals at 238,000. California has the greatest number at an estimated 71,000, and Texas has the next highest at 37,000.²³ Table 1 gives the estimated numbers of infected immigrants by state, and this information is represented graphically in Figure 3. The high prevalence of infection in the millions of Latin American immigrants in the US provides a convincing case for greater resource allocation in efforts to prevent and treat this disease.

Table 1: Estimated number of chagas cases and number of cases confirmed by blood screening by state²³

State	Est. Cases	AABB Cases	State	Est. Cases	AABB Cases
Alabama	1,116	8	Montana	46	1
Alaska	110	—	Nebraska	855	3
Arizona	6,440	28	Nevada	3,712	25
Arkansas	1,161	25	New Hampshire	159	3
California	70,860	707	New Jersey	8,686	32
Colorado	3,219	4	New Mexico	1,752	4
Connecticut	1,924	8	New York	17,403	160
Delaware	339	—	North Carolina	5,408	41
D.C.	745	2	North Dakota	23	1
Florida	18,096	260	Ohio	1,142	9
Georgia	5,681	37	Oklahoma	1,407	17
Hawaii	139	—	Oregon	1,995	13
Idaho	611	—	Pennsylvania	1,804	7
Illinois	9,316	22	Rhode Island	641	1
Indiana	1,705	12	South Carolina	1,486	15
Iowa	716	5	South Dakota	82	—
Kansas	1,273	9	Tennessee	1,900	14
Kentucky	618	9	Texas	36,977	176
Louisiana	1,427	15	Utah	1,767	24
Maine	49	1	Vermont	36	—
Maryland	5,926	29	Virginia	7,346	103
Massachusetts	3,346	9	Washington	3,144	18
Michigan	1,258	7	West Virginia	88	1
Minnesota	1,443	2	Wisconsin	1,239	3
Mississippi	434	11	Wyoming	112	—
Missouri	927	17	TOTAL	238,091	1,908

The AABB data included 6 confirmed infections whose state was unknown and 4 confirmed infections in Puerto Rico, not included in Table 1.

doi:10.1371/journal.pntd.0005033.t001

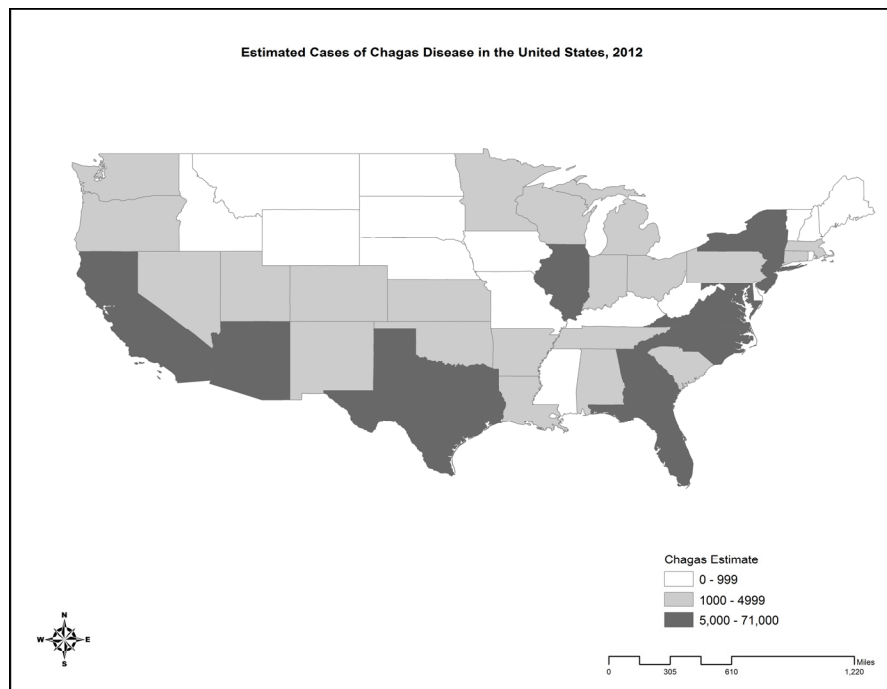


Figure 5: Distribution of estimated cases of Chagas disease by state.²³

Additionally, recent research has demonstrated a significant risk of autochthonous transmission in the southern US. As shown previously in Figure 4, several species of triatomine insects with high infections rates with *T. cruzi* inhabit southern regions of the United States.

Several cases of locally acquired infections have been identified in the US. In 2007, a 74-year-old woman living in Louisiana was bitten and infected after her house became infested with triatomine insects. The woman had traveled to regions with endemic Chagas disease but not in the past eight years.¹⁵ In 2012, analysis of blood donated through the American Red Cross and Blood Systems from 2006 to 2010 identified 16 cases of likely autochthonous transmission from around the US. Additionally, this study showed that 1 in 26,700 donors during this period had positive serological tests for *T. cruzi*.²⁴ In 2015, researchers examined 17 cases of Chagas disease identified by blood screening at the Gulf Coast Regional Blood Center in Houston. Of these 17, it was determined that five people with positive serological results for *T. cruzi* had likely been infected in Southeastern Texas.²⁵ In 2017, this same group used similar methods to identify an additional 11 cases of autochthonous Chagas transmission in South Central Texas.²⁶

In addition to the discovery of human infection in Texas, numerous cases of canine infection have been detected. From 1993-2007, 537 cases were confirmed by serology or histopathology.⁶ In Central America, infected dogs were determined to be important component of the disease cycle. Along with other mammals, dogs can act as reservoirs of *T. cruzi*. Unlike humans, dogs exhibit continuous parasitemia which gives

them a greater capability for transmitting the parasite to the insect vector. Past research has shown that the presence of infected dogs is a risk factor for human infection.²⁷

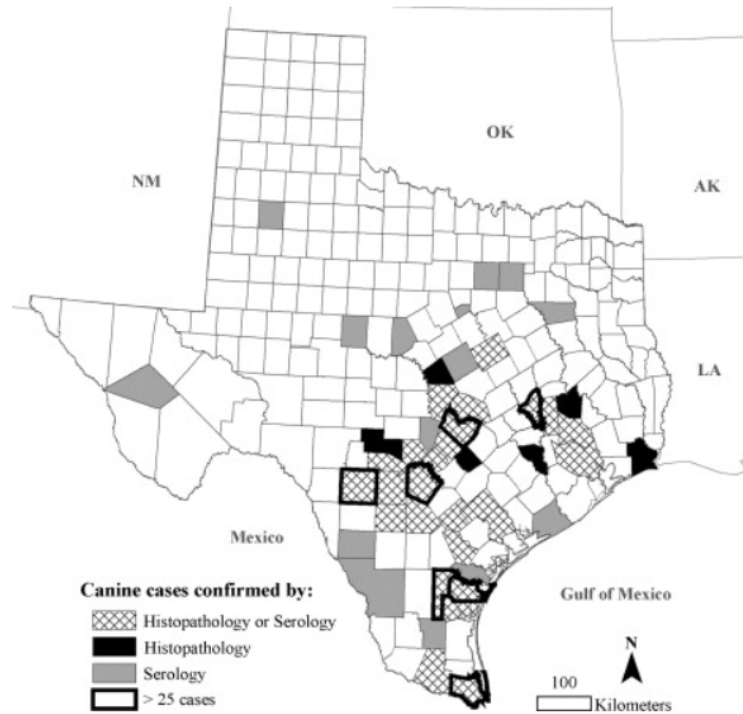


Figure 6: Distribution of confirmed canine infections in Texas.⁶

While the number of identified cases of locally acquired human infections is low, the number of risk factors present in the southern regions of the US merit some concern. The low visibility of the disease suggests that many autochthonous transmissions have gone undetected and that the approximately 35 cases that have been discovered are only a small portion of the local infections that have occurred. Additionally, environmental changes can affect insect behavior that could significantly increase the number of infections acquired in the US. For instance, hurricanes have been demonstrated to increase domestic infestation by triatomine insects.²⁸ Domestic infestation with triatomine insects is rare in the US, but the one reported case of autochthonous Chagas

transmission in Louisiana occurred immediately after hurricane Katrina in an infested home.¹⁵

Cruzipain

Considering significant morbidity and mortality associated with Chagas in Central and South America and the transmission risks in the US, new treatment options are urgently needed for Chagas disease. One avenue of research has been the inhibition of cruzipain, a cysteine protease present in *T. cruzi*. It is a member of the papain super family and is considered a cathepsin-L like enzyme due to structural similarities between the two cysteine proteases. Cruzain is a recombinant form of cruzipain utilized for this study.

Biological Roles of Cruzain

Cruzain is the most abundant protease and functions in many capacities in *T. cruzi*. Inhibition of cruzain interferes with the metacyclogenesis of *T. cruzi* from the replicative epimastigote form to the trypomastigote stage suggesting that it plays a role in cell remodeling.^{29,30} Additionally, cruzain facilitates host cell invasion by producing peptide ligands that activate bradykinin receptors. The resulting inflammation promotes the uptake of parasites in the bloodstream.^{31,32} Cruzain is also important for immune evasion. Macrophage activation is prevented by the interruption of the NF- κ B P65 pathway. NF- κ B P65 is colocalized with cruzain on the surface of the parasite and proteolytically cleaved.³³ Due to its importance in the life cycle of *T. cruzi*, inhibiting cruzain has been shown to cure *T. cruzi* infections in animal models making cruzain a validated target.^{34–36}

Cruzain Structure

Cruzain consists of two domains with the cleft between these domains forming a binding groove. The active contains the Cys25, His162, and Asn175 catalytic triad. This groove contains seven substrate binding subsites around the active site. S1-S4 bind the substrate on the acyl side of the cleavage point while S1'-S3' bind the substrate on the amino side. The S1 and S2 binding pockets play a significant role in positioning inhibitors at the active site. Figure 7 shows the crystal structure of cruzain, and Figure 8 shows the enzyme active site with the S1-S3 binding pockets labeled.

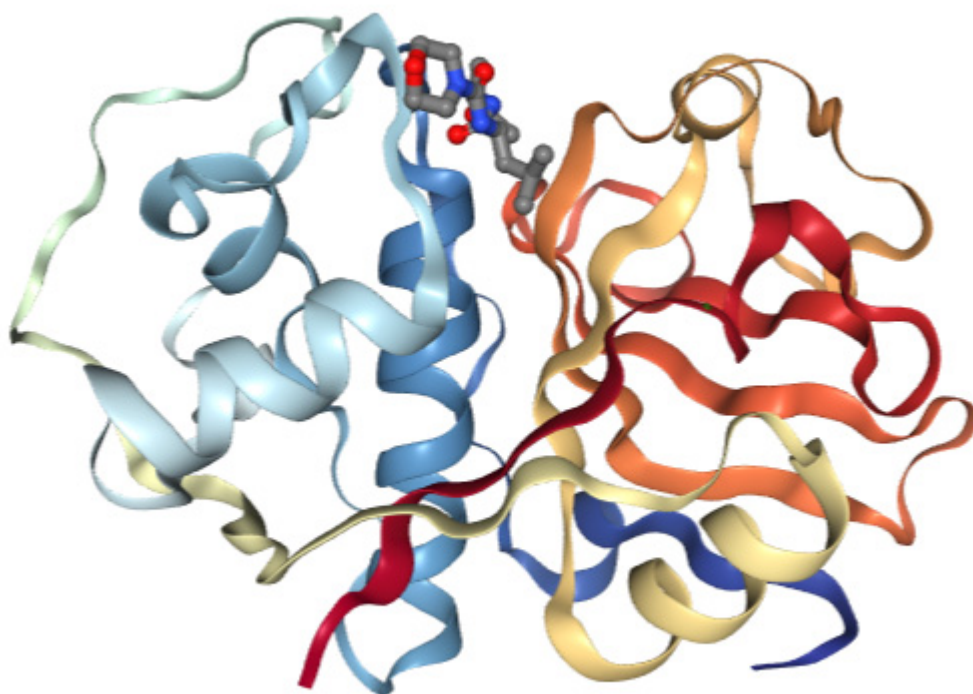


Figure 7: Cruzain crystal structure (PDB: 1EWP)

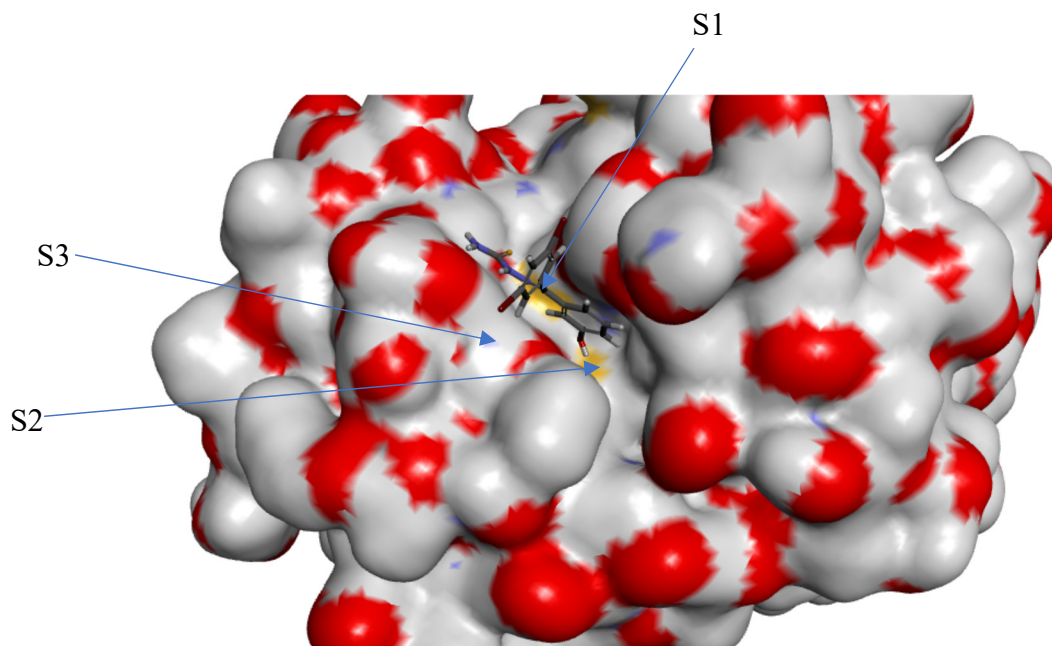


Figure 8: Cruzain complexed with a thiosemicarbazone inhibitor with substrate-binding subsites S1-S3 labeled (PDB:1ME3).³⁷

Table 2: Amino acid composition of mature cruzain.

AA	#	%	AA	#	%	AA	#	%
Ala	25	11.6	Ile	9	4.2	Arg	3	1.4
Cys	8	3.7	Lys	5	2.3	Ser	19	8.8
Asp	9	4.2	Leu	11	5.1	Thr	14	6.5
Glu	13	6.1	Met	4	1.9	Val	21	9.8
Phe	3	1.4	Asn	10	4.7	Trp	9	4.2
Gly	23	10.7	Pro	8	3.7	Tyr	7	3.3
His	4	1.9	Gln	10	4.7	Total	215	100

```

1   APAAVDWRARGAVTAVKDQGQCGSCWAFSAIGNVECQWFLAGHPLTNLSE
51  QMLVSCDKTDSGCSGGLMNNAFEWIVQENNGAVYTEDSYPYASGEGISPP
101 CTTSGHTVGATITGHVELPQDEAQIAAWLAVNGPVAVAVDASSWMTYTGG
151 VMTSCVSEQLDHGVLLVGYNDSAAVPYWIKNWTTQWGEEGYIRIAKGS
201 NQCLVKEEASSAVVG

```

Figure 9: Amino acid sequence of mature cruzain with active site residues highlighted (PDB: 1ME3).³⁷

```

1      MSGWARALLLA AVL VVMA CLVPAATASLHAEETLTSQFAEFKQKHGRVYESAAEEAFRLS
61     VFRENLFARLHAAANPHATFGVTPFSDLTREEFRSRYHNGAAHFAAAQERARVPVKVEV
121    VGAPAAVDWRARGAVTAVKDQGQCGSCWAFSAIGNVECQWFLAGHPLTNLSEQMLVSCDK
241    PQDEAQIAAWLAVNGPVAVAVDASSWMTYTGGVMTSCVSEQLDHGVLLVGYNDSAAVPYW
301    IIKNSWTTQWGEEGYIRIAKGSNQCLVKEEASSAVVGGPGPTPEPTTTTTTSAPGPSY
361    FVQMSCTDAACIVGCENVTLPTGQCLLTSGVSAIVTCGAETLTEEVFLTSTHCSGPSVR
421    SSVPLNKCNRLLRGSVEFFCGSSSSGRLADVDRQRRHQPYHSRHRRL

```

Figure 10: Amino acid sequence of preprocruzain. Legend: Green: Signal Peptide; Blue: Propeptide; Red: Mature Cruzain; Purple: C-Terminal.³⁸

Catalytic Mechanism of Cruzain

Recently, a new mechanism for the catalytic cleavage of peptides by cruzain was proposed by Zhai and Meek.³⁹ In this reaction, His162 acts as an acid and base, while the thiol group of Cys25 acts as a nucleophile. Until the substrate binds, Cys25 remains protonated with a pK_a of approximately 9.7. The presence of a peptide in the active site results in the deprotonation of Cys25 by His162 which allows the thiolate to act as a nucleophile. The result of the nucleophilic attack is a tetrahedral intermediate. The pi bond reforms with the loss of the amino side of the peptide. The resulting enzyme-peptide conjugate is then hydrolyzed.

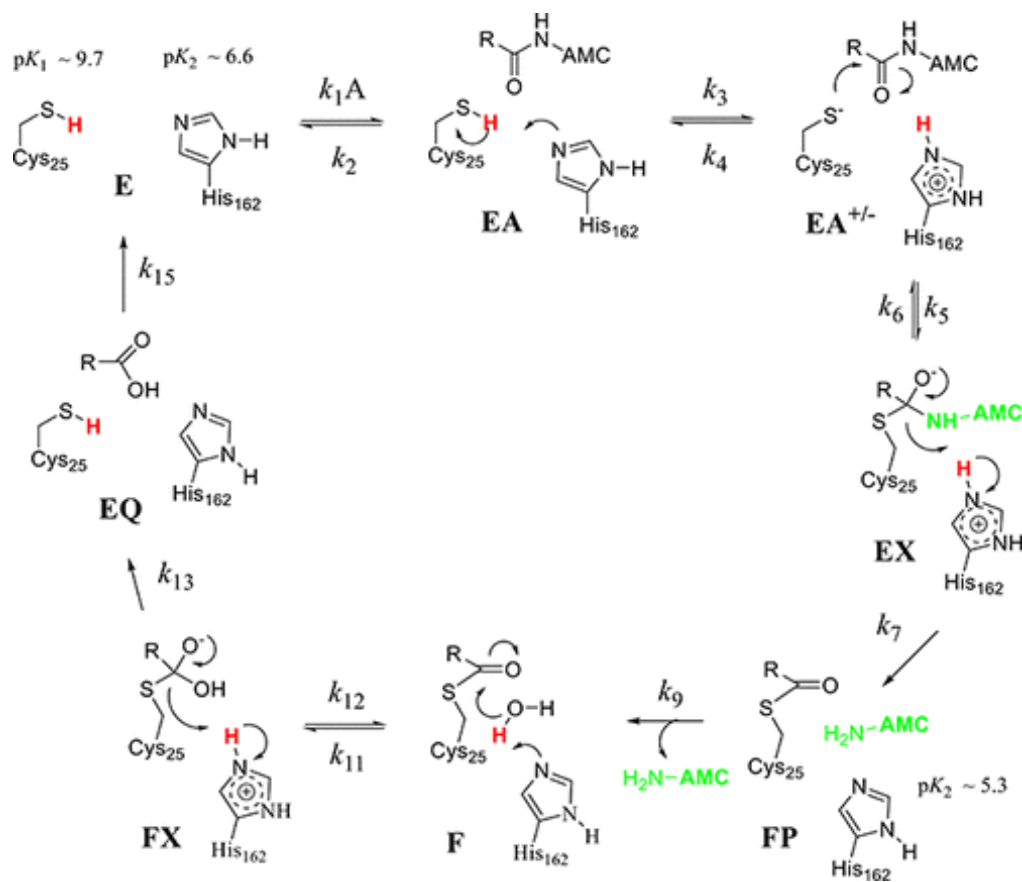


Figure 11: Catalytic mechanism of cruzain proposed by Zhai and Meek³⁹

CHAPTER TWO

Materials and Methods

Materials and Instrumentation

The kinetic characteristics of the inhibition of cruzain by thiosemicarbazone compounds were explored using fluorogenic assays. To enable fluorescence-based methods, a synthetic substrate of cruzain, 7-Amino-4-methylcoumarin, N-CBZ-L-phenylalanyl-L-arginine amide (Z-FR-AMC, Sigma) was used. When processed with cruzain, 7-amino-4-methylcoumarin (AMC) is cleaved from the substrate resulting in increased fluorescence ($\lambda_{\text{ex}}/\lambda_{\text{em}} = 355 \text{ nm}/460 \text{ nm}$). This fluorescence was measured using the Thermo Fluoroskan Ascent FI microplate reader. In each experiment, the reaction was carried out at a volume of 200 μL and in a black 96-well plate (Corning) like the one shown below. Cruzain DNA plasmid was donated to the Trawick group by Elizabeth Hansell and Dr. James McKerrow from the University of California at San Francisco, CA. Dr. Wara M. Arispe and Lauren Adamson expressed and purified the recombinant cruzain (1.1 μM).

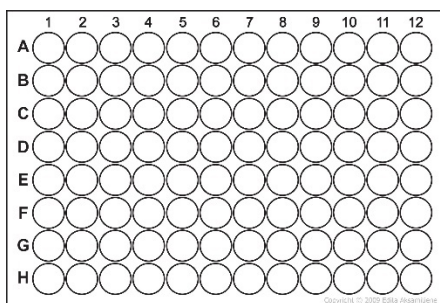


Figure 12: Layout of the 96-well plates used in the kinetic assays.

Preparation of stock solutions

Preparation of 400 mM, pH 5.5 sodium acetate buffer. Anhydrous sodium acetate was obtained from EMD (Lot #A0202224), and 1.3960 g of sodium acetate and 0.185 mL of glacial acetic acid were diluted to 45 mL with ultrapure water. The pH was adjusted using glacial acetic acid and 5 M sodium hydroxide, and the volume was then brought to a final 50 mL. The buffer was stored at 4 °C.

Preparation of 40 mM EDTA. Solid ethylenediaminetetraacetic acid (EDTA) was obtained from Omnipur (lot #0757B064), and 0.7444 g were diluted to 50 mL with ultrapure water. The EDTA stock solution was stored at 4 °C.

Preparation of 80 mM DTT. Solid dithiothreitol (DTT) was obtained from Omnipur (lot #1720C359), and 12.34 mg were diluted to 1 mL with 400 mM sodium acetate buffer. Since DTT is easily oxidized in water, this solution was prepared fresh for each experiment.

Preparation of 10% Brj-35. A 30% solution of Brj-35 solution was obtained from Sigma Aldrich (Lot #SLBC5854V), and 333 µL of the 30% Brj-35 solution were diluted to 1 mL with ultrapure water.

Preparation of 6 mM Z-FR-AMC and 6 mM AMC. Solid Z-FR-AMC was obtained from Sigma Aldrich and 3.90 mg were diluted to 1 mL in 99% dimethyl sulfoxide (DMSO) (Corning). Solid AMC was obtained from Anaspec, and 1.05 mg were diluted to 1 mL with 99% DMSO.

Preparation of 20 mM KGP compound solutions. Thiosemicarbazone inhibitors were synthesized by members of the Dr. Kevin G. Pinney laboratory. These inhibitors

were obtained as 20 mM stock solutions in 99% DMSO. Serial dilutions of these 20 mM stocks were performed with 99% DMSO to get solutions A-F for each solution which had concentrations of 2 mM, 200 μ M, 20 μ M, 2 μ M, 200 nM, and 20 nM respectively. These dilutions are outlined in Table 3.

Table 3: Preparation of inhibitor stocks A-F

	[I]	μ L Previous sol	100 % DMSO (μ L)	Total (μ L)
Stock	20 mM			
A	2 mM	20	180	200
B	200 μ M	20	180	200
C	20 μ M	20	180	200
D	2 μ M	20	180	200
E	0.2 μ M	20	180	200
F	0.02 μ M	20	180	200

Preparation of Assay Solutions and Final Assay Conditions

Before each experiment, an assay buffer, an enzyme buffer, inhibitor solutions, and substrate solutions were made from the stock solutions described previously. The assay buffer consisted of 130 mM sodium acetate, 1.3 mM EDTA, 3.25 mM DTT, and 0.013% Brj-35. Table 3 shows the quantities of stock solutions used to prepare various volumes of assay buffer. The enzyme buffer consisted of 100 mM sodium acetate, 1 mM EDTA, 2.5 mM DTT, and 0.29 nM cruzain. Table 4 shows the quantities of stock solutions used to prepare various volumes of the enzyme buffer. Inhibitor solutions consisted of various concentrations of inhibitor in 35% DMSO and ultrapure water. The formulation of inhibitor solutions with various concentrations from inhibitor stocks A-F is shown in Table 5. Substrate solutions of various concentrations were obtained by

serial dilutions of the 6 mM stock with water and DMSO so that the final DMSO concentration of each solution was 2.5 %. These serial dilutions are outlined in Table 6.

Table 4: Assay Buffer Preparation

Total Volume (μL)	Volume needed (μL)	EDTA (μL)	DTT (μL)	NaOAc (μL)	Water (μL)	Brj (μL)
1000	800	32.5	40.63	325	600.6	1.3
2000	1600	65	81.25	650	1201	2.6
3000	2400	97.5	121.9	975	1801	3.9
4000	3200	130	162.5	1300	2402	5.2
5000	4000	163	203.1	1625	3003	6.5
6000	4800	195	243.8	1950	3603	7.8
7000	5600	228	284.4	2275	4204	9.1
8000	6400	260	325	2600	4805	10.4
9000	7200	293	365.6	2925	5405	11.7
10000	8000	325	406.3	3250	6006	13
11000	8800	358	446.9	3575	6606	14.3
12000	9600	390	487.5	3900	7207	15.6

Table 5: Enzyme buffer preparation

Total Volume (μL)	Volume needed (μL)	EDTA (μL)	DTT (μL)	NaOAc (μL)	Water (μL)	Brj (μL)	Cruzain (μL)
600	560	15	18.8	150	415.5	0.6	0.16
1200	1120	30	37.5	300	831	1.2	0.31
1800	1680	45	56.3	450	1247	1.8	0.47
2400	2240	60	75	600	1662	2.4	0.62
3000	2800	75	93.8	750	2078	3	0.78
3600	3360	90	113	900	2493	3.6	0.94
4200	3920	105	131	1050	2909	4.2	1.09
4800	4480	120	150	1200	3324	4.8	1.25
5400	5040	135	169	1350	3739	5.4	1.40
6000	5600	150	188	1500	4155	6.0	1.56
6600	6160	165	206	1650	4570	6.6	1.72
7200	6720	180	225	1800	4986	7.2	1.87

Table 6: Preparation of inhibitor solutions. The final [I] indicates the concentration of inhibitor on the reaction solution

Final [I]	[I] μ M	Solution	μ L	DMSO	Water
20	400	Stock	2	33	65
10	200	A	10	25	65
5	100	A	5	30	65
1	20	B	10	25	65
0.5	10	B	5	30	65
0.1	2	C	10	25	65
0.05	1	C	5	30	65
0.01	0.2	D	10	25	65
0.001	0.02	E	10	25	65
0.0005	0.01	E	5	30	65
0.0001	0.002	F	10	25	65
0.00005	0.001	F	5	30	65
0.00001	0.0002	F	1	34	65

Table 7: Preparation of substrate solutions. Final [S] indicates the concentration of substrate in the reaction solution.

Final [S] (μ M)	[S] (μ M)	6 mM Stock (μ L)	Previous Sol (μ L)	DMSO (100%) (μ L)	Water (μ L)
15	150	25		0	975
10	100		666.7	8.3	325
7.5	75		750	6.3	243.7
5	50		666.7	8.3	325
2.5	25		500	12.5	487.5
1	10		400	15	585
0.75	7.5		750	6.3	243.7
0.5	5		666.7	8.3	325

Kinetic studies were carried out in 100 mM sodium acetate buffer (pH 5.5) with 1 mM EDTA, 2.5 mM DTT, 2% DMSO, and 0.01% Brj-35. The enzyme concentration was 0.1 nM and the substrate (Z-FR-AMC) concentration was 15 μ M unless otherwise specified. These conditions were attained by combining 100 μ L of assay buffer, 70 μ L of

enzyme solution, 10 μL of inhibitor solution, and 20 μL of substrate solution in each 200 μL well.

Experimental Methods

Obtaining an AMC Standard Curve

The fluorescence values obtained in these experiments were unitless, relative measurements. Therefore, it was necessary to measure the fluorescence of 7-amino-4-methylcoumarin at a variety of concentrations to obtain a standard curve. Columns 1-3 on a 96-well plate each contained eight solutions of AMC at eight different concentrations. These concentrations were 15 μM , 10 μM , 7.5 μM , 5.0 μM , 2.5 μM , 1.0 μM , 0.75 μM , 0.5 μM . The solutions also contained DTT, EDTA, Brj-35, and sodium acetate buffer at the previously described concentrations. The fluorescence of each well was then measured using the Fluoroskan Ascent Fl. The resulting fluorescence values were then plotted against the concentration values to give a standard curve. Since the relationship between AMC concentration and fluorescence was linear, this curve yielded a linear equation that allowed the determination of the change in AMC concentration in later experiments.

Determination of K_M , k_{cat} , and V_{max}

To quantify the kinetic parameters of the cleavage of Z-FR-AMC by cruzain, the rate of cleavage was measured at substrate concentrations of 15 μM , 10 μM , 7.5 μM , 5 μM , 2.5 μM , 1 μM , 0.75 μM , and 0.5 μM . As soon as the substrate was added, fluorescence was measured every 15 seconds for 5 minutes. To determine the reaction velocities, the fluorescence values were converted to AMC concentrations using the previously obtained standard curve. The AMC concentrations were then plotted against

time, and reaction velocity was determined by linear regression. The reaction velocities were then plotted against the substrate concentrations, and a Michaelis-Menten curve was fitted to the data using GraphPad to give K_M , k_{cat} , and V_{max} .

Determination of Inhibition by Thiosemicarbazone Compounds at 10 μ M

To quickly measure the effectiveness of multiple thiosemicarbazone inhibitors, the percent inhibition for each compound was measured at an inhibitor concentration of 10 μ M. Eight wells contained no inhibitor, and four wells per compound contained 10 μ M inhibitor. The enzyme and inhibitor were pre-incubated for 5 minutes at 25 °C before the substrate was added and the rate of change in fluorescence was measured. The uninhibited reaction rate was determined by averaging the linear regression for the fluorescence versus time data in each control well. The rate for the inhibited reactions was determined the same way. Comparing the rate of the reaction in uninhibited wells to the rate of the reaction in the presence of inhibitor allowed the calculation of percent inhibition. Compounds that decreased the reaction rate by more than 50% were further characterized by additional experiments while those that decreased the rate by less than 50% were considered ineffective inhibitors.

Measurement of IC_{50} Values

Compounds which inhibited cruzain by more than 50% at 10 μ M were further characterized by determining the concentration of the compound was required to inhibit cruzain by 50%. To do so, the enzyme was incubated with the compound at eight different inhibitor concentrations (50 pM to 10 μ M) for 5 minutes at 25 °C. Substrate was then added to each of these mixtures, and fluorescence was measured every 15 seconds for 5 minutes. A linear regression of the fluorescence versus time data gave the

reaction rate for each inhibitor concentration. This reaction rate was converted to fractional activity by dividing the rates by the average rate of the uninhibited reaction. The fractional activity was then plotted against the logarithm of the inhibitor concentration. The data followed a sigmoidal dose response, and equation 1 was used to determine the IC_{50} by non-linear regression. This analysis was performed in GraphPad.

$$y = \text{Bottom} + \frac{(\text{Top} - \text{Bottom})}{1 + 10^{(\log IC_{50} - x) * \text{HillSlope}}} \quad \text{Eq. 1}$$

Determination of Time-Dependence of KGP434

For the most potent inhibitor, KGP434, additional experimentation was performed to determine if its inhibition of cruzain is time-dependent. Eight different inhibitor concentrations were used (10 μM , 1 μM , 0.1 μM , 100 nM, 50 nM, 10 nM, 5 nM, 500 pM, 50 pM), and three identical sets of reaction mixtures were prepared with a substrate concentration of 15 μM . The reaction was initiated without any preincubation of the enzyme and inhibitor. Fluorescence was measured every 15 seconds for one hour. The results were used to make progress curves of fluorescence versus time which indicated whether inhibition at a given inhibitor concentration was time-dependent or not.

Determination of the Mode of Inhibition by KGP434

Progress curves were obtained using a procedure like the one described for determining time-dependence. The only difference was that multiple substrate concentrations were used while the inhibitor concentration was fixed at 1 μM . The substrate concentrations used were 15 μM , 10 μM , 7.5 μM , 5 μM , 2.5 μM , 1 μM , 0.75 μM , and 0.5 μM . The resulting progress curves were used to obtain a k_{obs} by fitting equation 2 to the data using GraphPad.

$$S = v_s t \frac{(v_o - v_s)}{k_{obs}} (1 - e^{-k_{obs} t}) \quad \text{Eq. 2}$$

Determination of Reversibility for KGP434

In this assay, cruzain and KGP434 were incubated at high concentrations for one hour to ensure that the enzyme was fully inhibited. This incubation solution was then diluted one hundred-fold. If an inhibitor is reversible, it is expected to disassociate over time resulting in a recovery of enzyme activity. If it is irreversible, no disassociation would be expected and the activity would remain the same. Cruzain, at a concentration of 10 μM , was incubated with KGP434 at concentrations of 5 μM and 1.7 μM which is 100 times the IC_{50} concentration for this inhibitor. After a one-hour incubation, the incubation solution was diluted 100-fold so that the reaction conditions would be as listed in the introduction to this chapter. This was done by adding 2 μL of each incubation solution to a well on a 96-well plate and then adding 198 μL of dilution buffer (prepared according to the table below). The progress of the reaction was then measured by taking fluorescence readings every 4 seconds for 1000 measurements. A more detailed protocol can be found in Appendix B.

Table 8: Dilution buffer components

Total Volume	EDTA	DTT	H ₂ O	NaOAc	6 mM substrate	Brj
1800 μl	45 μl	56.25 μl	1202 μl	450 μl	45 μl	1.8 μl

CHAPTER THREE

Results and Discussion

AMC Standard Curve

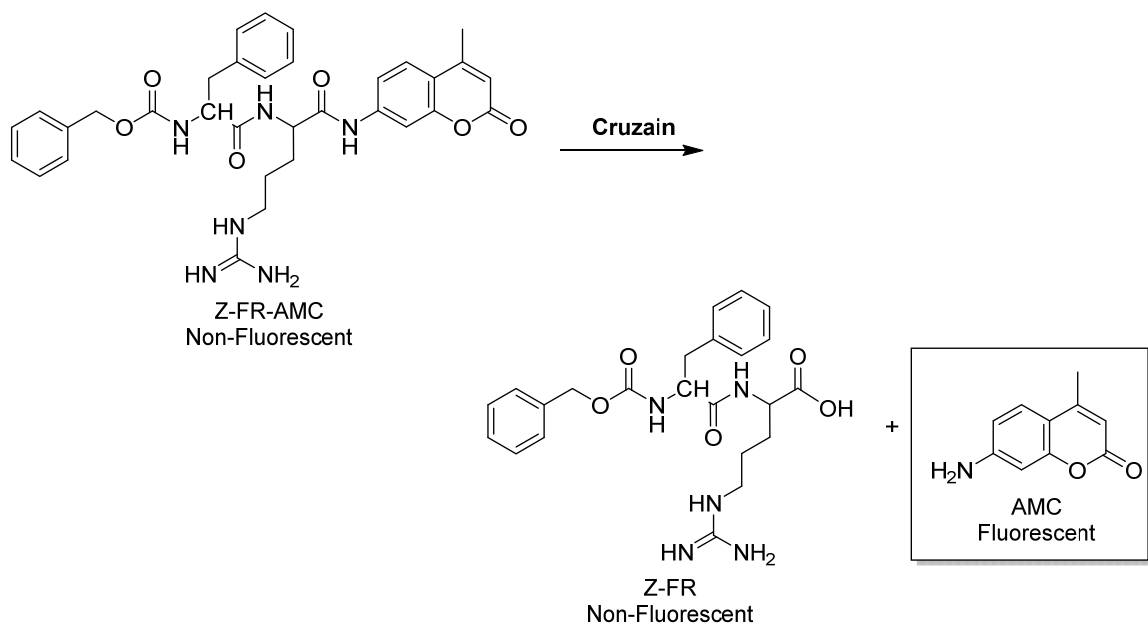


Figure 13: Z-FR-AMC cleavage by cruzain

All cruzain assays were performed using the synthetic substrate Z-FR-AMC (Figure 13). When cleaved from the substrate by cruzain, AMC is highly fluorescent which makes it possible to track the progress of the reaction using fluorometric techniques. However, in order to objectively measure the rate of the reaction as an amount of AMC cleaved from the substrate, it was necessary to relate the concentration

of AMC to the level of fluorescence observed. This was done by creating a standard curve of fluorescence versus AMC concentration which is shown in Figure 14.

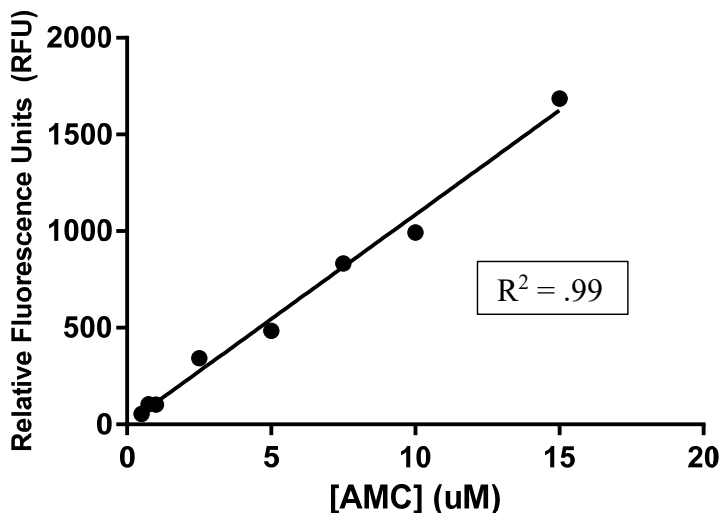


Figure 14: Standard curve of fluorescence versus AMC concentration.

Cruzain – Z-FR-AMC Kinetics

Since the measurements of inhibitor efficacy were performed using a synthetic substrate, it was necessary to characterize the affinity of the substrate for cruzain. The reaction velocity at different substrate concentrations was measured by taking the slope of a linear regression of the data for fluorescence versus time (Figure 15). These velocities were plotted against concentration, and the Michaelis-Menten equation was used to fit a curve to the data which yielded the V_{\max} , K_m and k_{cat} . These values, shown in Figure 16, indicated a high affinity of the substrate for cruzain which was necessary to meaningfully quantify the effectiveness of different inhibitors. Additionally, comparison

of these values to literature values for cruzain indicated that the enzyme was sufficiently active for use in kinetic assays.

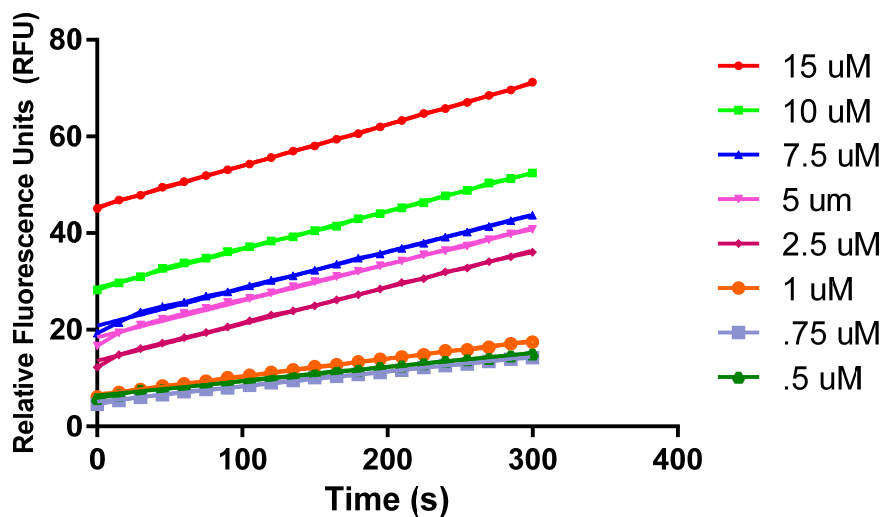


Figure 15: Fluorescence versus time for multiple reactions with varying concentrations of substrate.

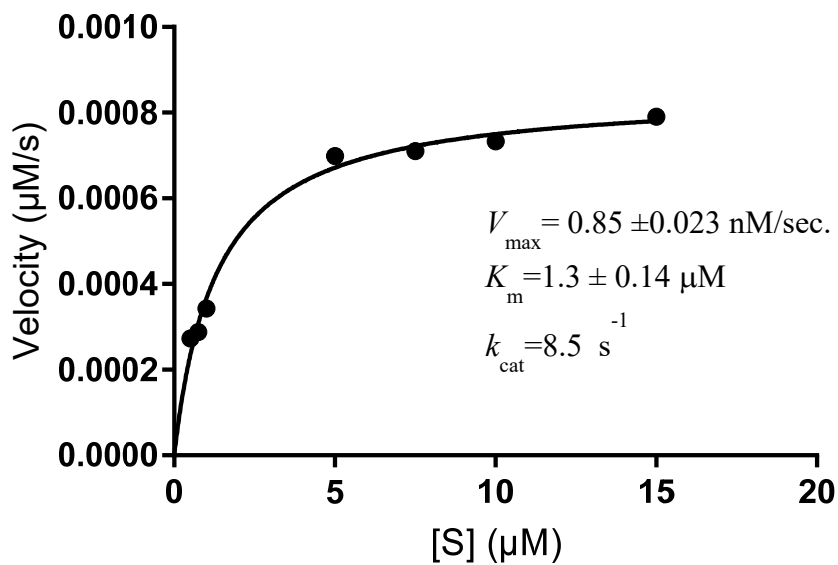


Figure 16: Michaelis-Menten curve of cruzain with Z-FR-AMC substrate.

Work Flow for Inhibitor Screening and Characterization

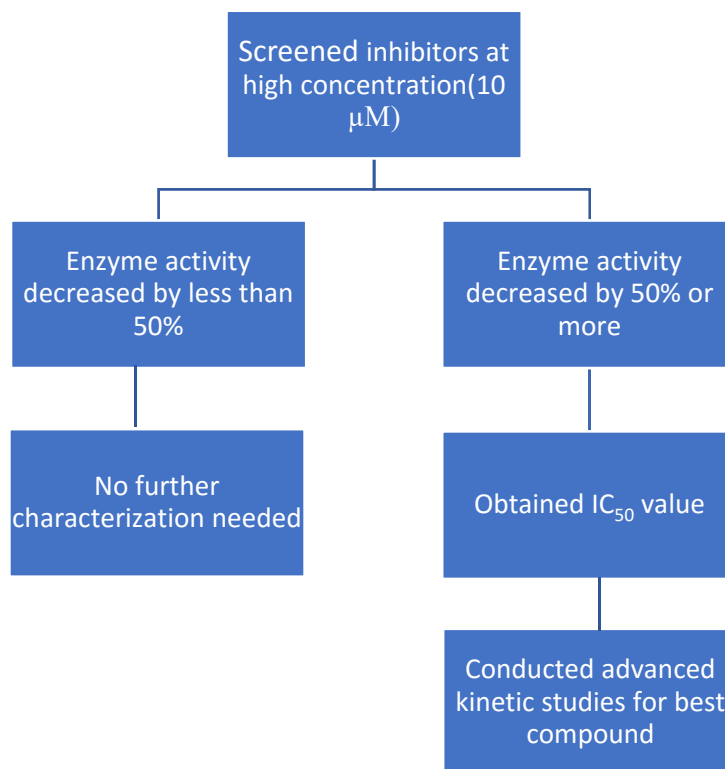


Figure 17: Workflow for inhibitor screening a characterization

High Concentration Screening of Inhibitors and Determination of IC₅₀ Values

After establishing that the synthetic substrate was appropriate, a library of 20 small-molecule, thiosemicarbazone containing inhibitors were tested against cruzain using a high concentration of the inhibitor (10 μM). This process allowed for efficient screening of the library of compounds to identify inhibitors that might be effective at low concentrations. Those compounds that decreased enzyme activity by less than 50% at this concentration were considered relatively ineffective and no additional tests were performed.

Inhibitors that decreased enzyme activity by greater than 50% at this concentration were further characterized by obtaining IC₅₀ values. The decrease in enzyme activity was measured at several different inhibitor concentrations and equation 1 was used to obtain an IC₅₀ value. Figure 18 shows an example of a graph of fractional activity versus the logarithm of the inhibitor concentration (KGP434 in this case) which was used to obtain the IC₅₀. Table 4 shows the results of the 10 µM test and (when applicable) the IC₅₀ values obtained for each compound.

$$y = \text{Bottom} + \frac{(\text{Top}-\text{Bottom})}{1+10^{(\log \text{IC}_{50}-x) \cdot \text{HillSlope}}} \quad \text{Eq. 1}$$

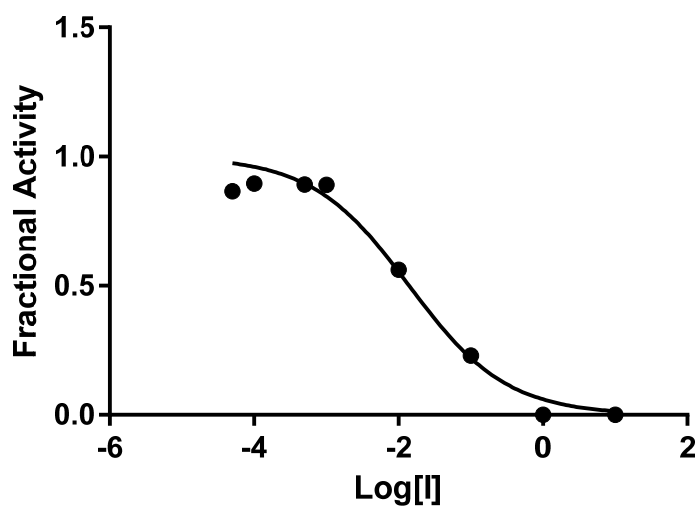
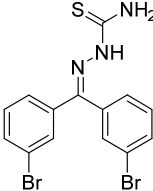
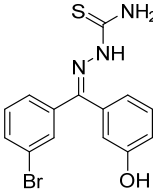
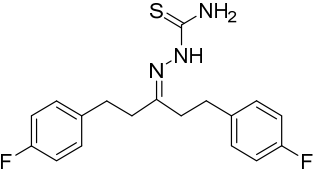
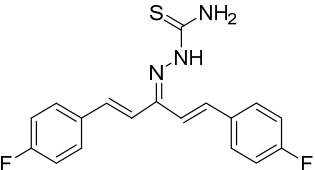
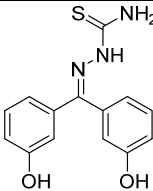
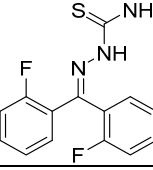
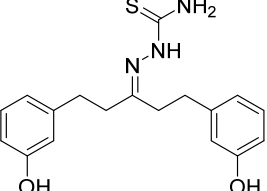
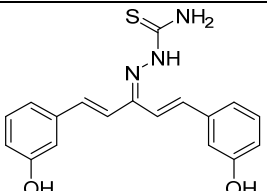
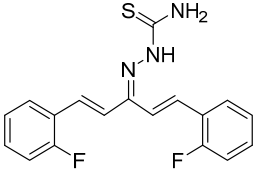
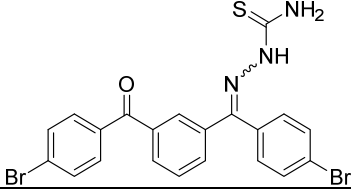
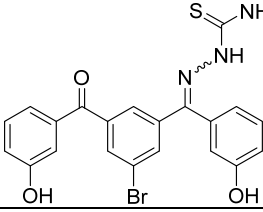
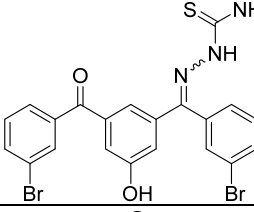
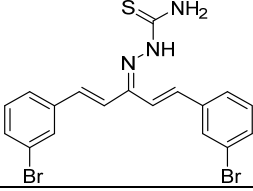
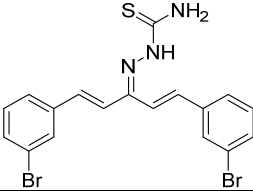
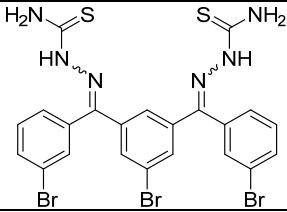
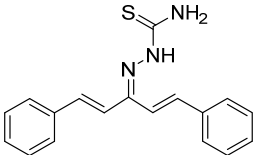
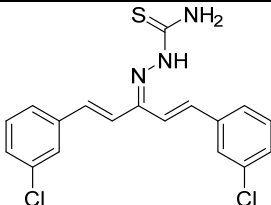
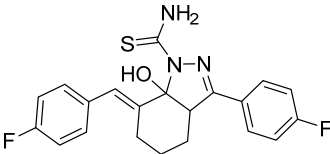
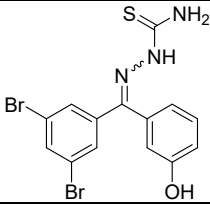
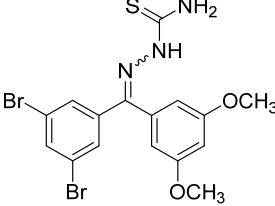
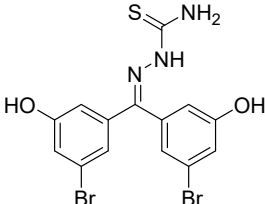


Figure 18: Fractional activity plotted against the log of the inhibitor concentration allows for determination of the IC₅₀.

Table 9: Compound structure and IC₅₀ values (see Erica Parker's Dissertation for more structure syntheses⁴⁰)

Compound	Structure	IC ₅₀
KGP68 ⁴¹		28.5 nM
KGP94 ⁴²		211.9
KGP364		> 10 μM
KGP365		> 10 μM
KGP381		> 10 μM
KGP382 ⁴³		427.1 nM
KGP383		< 10 μM, IC ₅₀ ND
KGP384		2.78 μM

KGP385		445.2 nM
KGP388 ⁴⁴		565.4 nM
KGP402 ⁴⁴		29.7 nM
KGP403 ⁴⁴		< 10 μ M, IC ₅₀ ND 81.1% inhibition at 10 μ M
KGP404		< 10 μ M, IC ₅₀ ND 78.8% inhibition at 10 μ M
KGP405		> 10 μ M
KGP406		679.5 nM
KGP421		487.9 nM

KGP422		> 10 μ M
KGP431		> 10 μ M
KGP434 ⁴⁵		17.0 nM
KGP435 ⁴⁵		64.3 nM
KGP451 ⁴⁵		94.3 nM

Initial screening of inhibition at high concentration of inhibitor eliminated six compounds from further consideration. KGP68 showed excellent inhibition of cruzain but exhibited very poor solubility in aqueous solutions. Several related compounds (KGP94, KGP434, KGP435, and KGP451) were also identified as good inhibitors and were significantly more soluble. KGP402 has a significantly different structure than most of the other effective inhibitors but had one of the lowest IC₅₀'s and certainly merits further testing.

Advanced Kinetic Studies of KGP434

With an IC_{50} of 17 nM, KGP434 is clearly a potent inhibitor. In in vitro assays, it inhibited cruzain slightly more effectively than did KGP68, a previous lead compound with many structural similarities. Moreover, KGP68 was hindered in later testing by its relative insolubility in aqueous solutions, but KGP434 contains a hydroxyl substituent which significantly increases its solubility. These promising characteristics justified additional characterization of the qualities of this inhibitor.

First, an assay was performed to determine if the binding of KGP434 was time-dependent. Time dependent inhibitors bind slowly relative to the rate of enzyme turnover. Time dependent inhibition typically implies a slow rate of disassociation of the enzyme and inhibitor or irreversible inhibition. This can be a positive characteristic in therapeutic agents since a slow k_{off} can result in longer lasting effect at low concentrations due to longer inhibitor residence time.⁴⁶ This assay was performed by observing the reaction progress in the presence of 15 μ M substrate and with several different inhibitor concentrations. The enzyme and inhibitor were not preincubated, so, if time dependent, enzyme activity should clearly decrease over time after the start of the reaction. Additionally, the initial velocities should be similar regardless of the inhibitor concentration. Figure 19 shows the results of this assay and confirm a time-dependent mode of inhibition. Depending on the inhibitor concentration, inhibition continually increased for a duration of several minutes up to nearly an hour. Despite being the quickest to reach the maximum level of inhibition, the reaction with inhibitor concentration of 10 μ M still required several minutes to reach the maximal inhibition which is slow on the time-scale of enzymatic turnover.

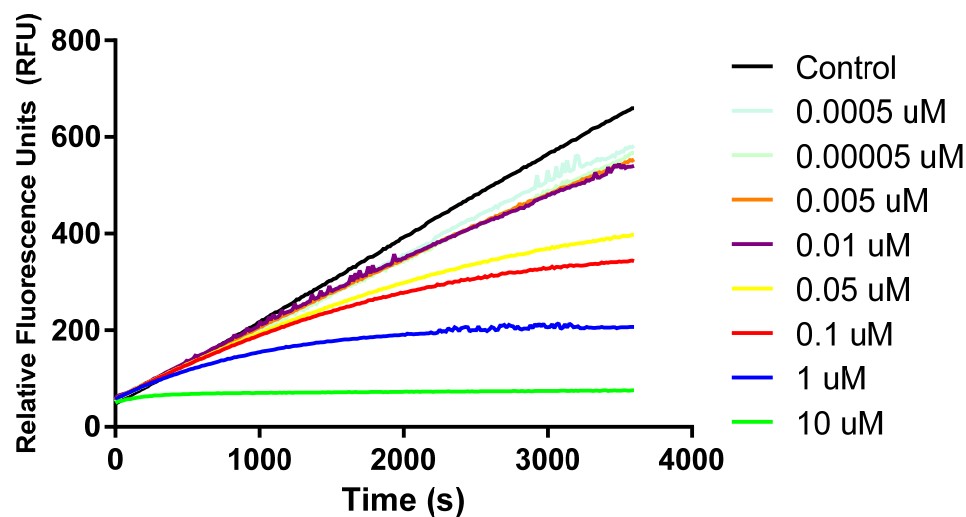


Figure 19: Progress curve of cruzain in the presence of increasing concentrations of KGP434, demonstrating a time-dependent mode of inhibition.

Having established time dependence, it was possible to determine the KGP434's mode of action by calculating the k_{obs} values from a similar assay using a fixed inhibitor concentration and varying the substrate concentration. Again, the reaction was started without preincubating the enzyme and inhibitor. Figure 20 shows the progress curves generated by this assay. These progress curves were then used to calculate k_{obs} , a rate constant which characterizes the transition between the initial reaction velocity and the steady state velocity. For competitive time-dependent inhibitors, k_{obs} decreases hyperbolically as substrate concentration increases. For non-competitive inhibitors, k_{obs} increases hyperbolically as substrate concentration increases. For uncompetitive inhibitors, k_{obs} is independent of substrate concentration.⁴⁶ For KGP434, k_{obs} was calculated using equation 2 where S is substrate concentration (μM), v_s is steady state velocity, t is time (s), v_o is initial velocity. Figure 21 shows the plot of k_{obs} vs substrate concentration which was consistent with the competitive mode of inhibition.

$$S = v_s t \frac{(v_o - v_s)}{k_{obs}} (1 - e^{-k_{obs} t}) \quad \text{Eq. 2}$$

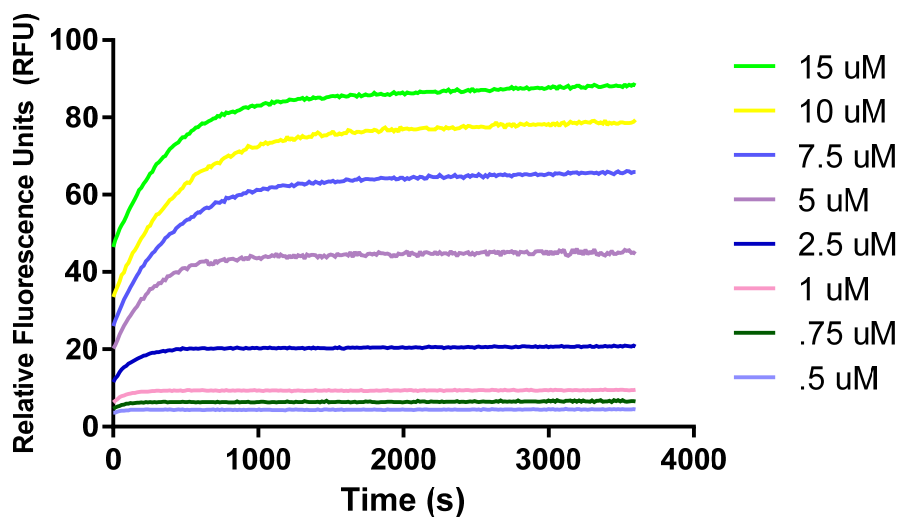


Figure 20: Increasing inhibition of cruzain was observed with decreasing substrate concentrations in the presence of KGP434 (1 μ M).

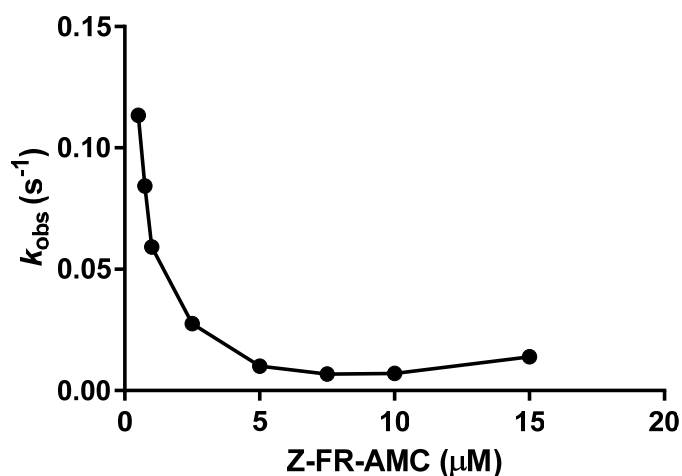


Figure 21: k_{obs} vs. substrate concentration. The shape of the plot indicates that both inhibitor (KGP434) and substrate compete for the same site.

As discussed previously, time-dependent inhibition frequently indicates irreversible inhibition or slowly-reversible inhibition. To determine if KGP 434 inhibited cruzain reversibly, the inhibitor and enzyme were incubated for one hour at high concentrations. The incubated inhibitor and enzyme were then diluted in a solution

containing substrate and the reaction progress was measured for 4000 seconds. Figure 22 shows the results of this experiment. The enzyme in the solution containing KGP434 with a concentration of 17 nM initially exhibited 18.1% of the activity of the control solutions which did not contain any inhibitor. At the end of the experiment, the activity had increased to 29.7% of the activity in the control solutions. The enzyme in the solution containing KGP434 with a concentration of 50 nM initially exhibited an 12.2% of the activity of the control solutions which did not contain any inhibitor. At the end of the experiment, the activity had increased to 23.5% of the activity in the control solutions. The moderate increase in enzyme activity over the course of about an hour provides clear evidence that KGP 434 inhibits cruzain reversibly.

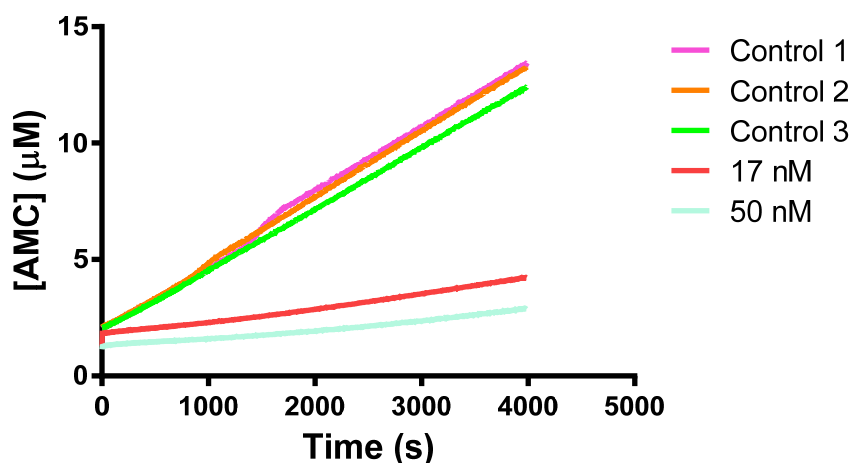


Figure 22: Reversibility study of KGP434

Molecular Modeling

Molecular modeling is a valuable tool for determining the likely orientation of the inhibitor in the active site of an enzyme. This modeling was performed using Discovery Studio 2016 Client. Many possible conformations were analyzed, and the most likely conformation was chosen based on having the highest relative interaction energy. This

conformation, shown in Figure 23, shows that when the dibromophenyl group is positioned in the S3 pocket and the hydroxyphenyl group is in the deep, hydrophobic S2 pocket, the thiosemicarbazone moiety is positioned near the sulfur of Cys25 side-chain. This proximity suggests the possibility of a covalent modification of the enzyme.

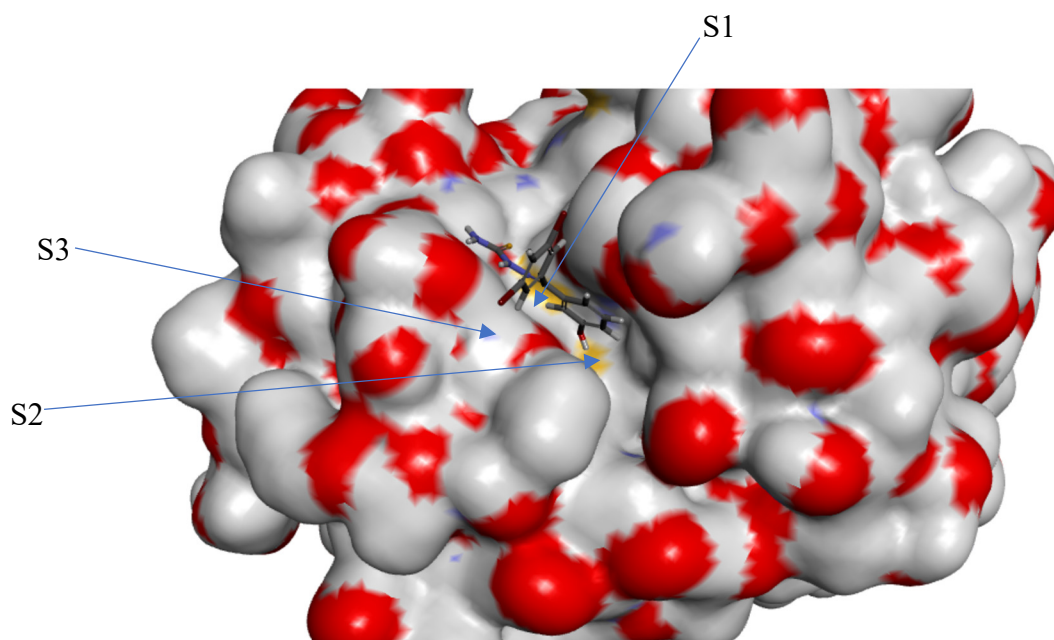


Figure 23: Molecular model of KGP434 bound to cruzain (PDB:1ME3)³⁷

Proposed Mechanism of Inhibition

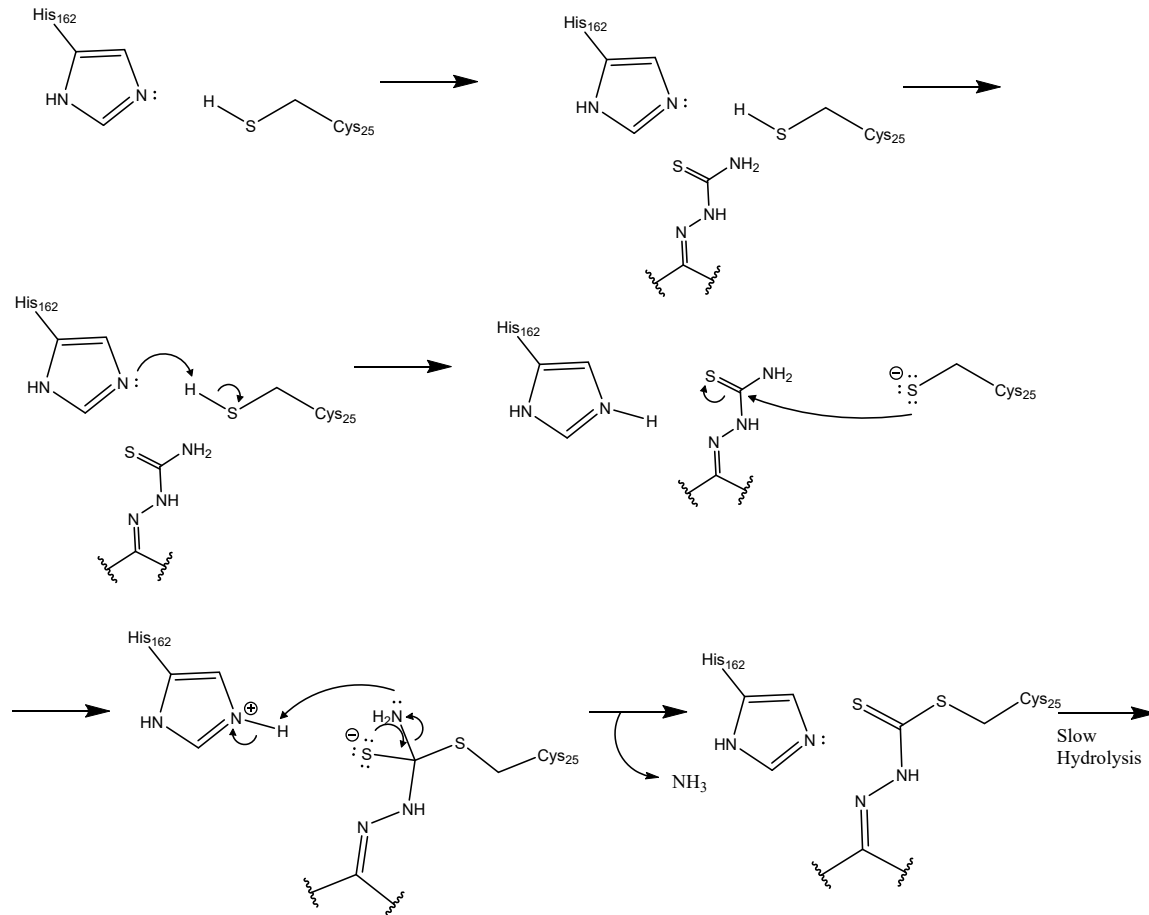


Figure 24: Proposed mechanism for the covalent inhibition of cruzain by KGP434

Based on the proximity of the thiosemicarbazone moiety to the sulfur of Cys25 in the active site of cruzain, a covalent mechanism was proposed as shown in Figure 24.³⁹ This mechanism involves a nucleophilic attack by the cysteine thiol resulting in a tetrahedral intermediate. The carbon-sulfur double bond reforms, and an ammonium ion leaves. This covalently bonded inhibitor would likely undergo non-enzyme directed hydrolysis resulting in the slowly-reversible inhibition observed in the kinetic studies.

Conclusions

Thiosemicarbazone library screening at high inhibitor concentration. Screening the library of 20 thiosemicarbazone compounds eliminated six compounds from further consideration (KGP364, 365, 381, 506, 422, 431). These compounds had IC_{50} values greater than 10 μ M.

IC_{50} Determination. KGP68 showed excellent inhibition of cruzain but exhibited very poor solubility in aqueous solutions. Several related compounds (KGP94, KGP434, KGP435, and KGP451) were also identified as good inhibitors and were significantly more soluble. KGP402 has a significantly different structure than most of the other effective inhibitors but had one of the lowest IC_{50} 's (29.7 nM) and certainly merits further testing. KGP 434 had the lowest IC_{50} (17.0 nM). Its structure is similar to that of KGP68, but a hydroxyl substitution on one of the aryl rings significantly increases its solubility. Due to its low IC_{50} and good solubility, advanced kinetic studies were performed to further characterize KGP434.

Advanced Kinetic Studies of KGP434. An assay to determine the change in cruzain reaction velocity over time at different inhibitor concentrations showed that KGP434 inhibits cruzain a time-dependent manner. A similar assay was performed with fixed inhibitor concentration and varying substrate concentrations. The data from this assay was used to calculate k_{obs} , the rate constant for the conversion of initial velocity to steady state velocity, which showed that k_{obs} decreased hyperbolically as inhibitor concentration increased. This was consistent with competitive inhibition. Finally, a reversibility study was performed by incubating the inhibitor and enzyme at high concentrations before performing a 100-fold dilution and initiating the reaction. The

reaction velocity was observed to increase over time which indicated a recovery of enzyme activity which implies that KGP434 inhibits cruzain reversibly.

Molecular Modeling. Molecular modeling indicated that the likely conformation of KGP434 in the active involved the positioning of the dibromophenyl group in the S3 pocket, the hydroxyphenyl group in the deep, hydrophobic S2 pocket, and the thiosemicarbazone moiety near the thiol group of Cys25. This proximity suggests the possibility of a covalent modification of the enzyme.

APPENDIX A

Additional Data

Results of IC_{50} Assays

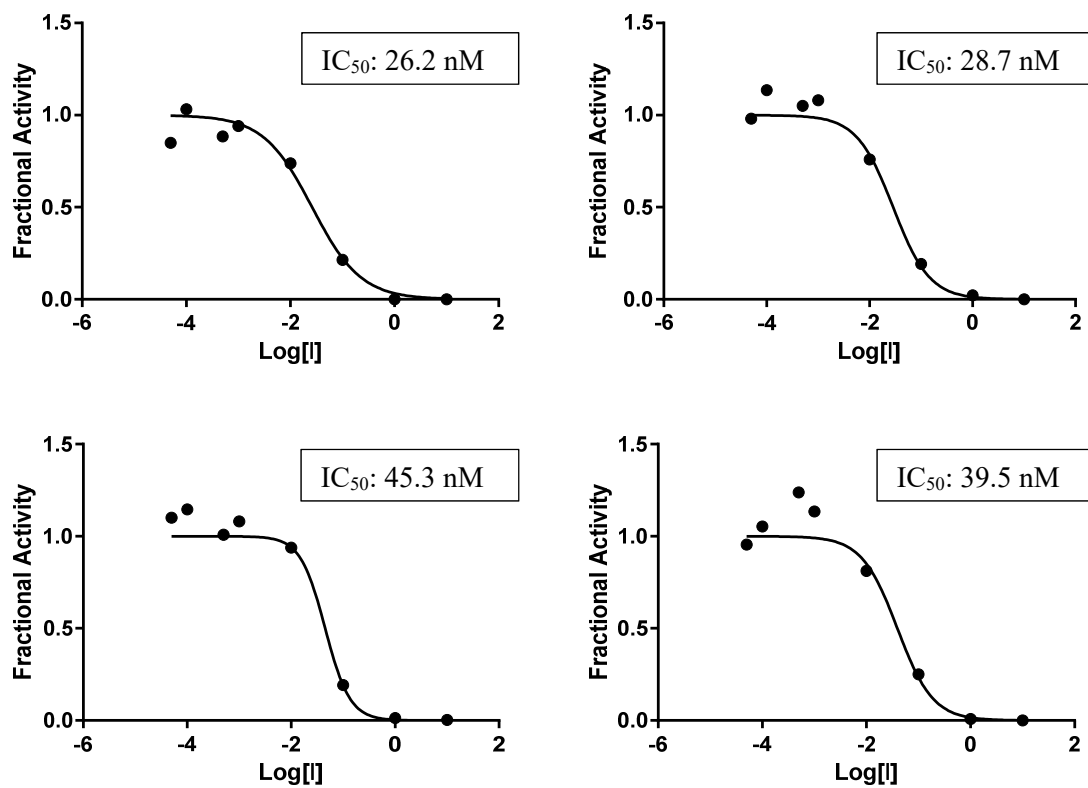


Figure 25: IC_{50} results for KGP68

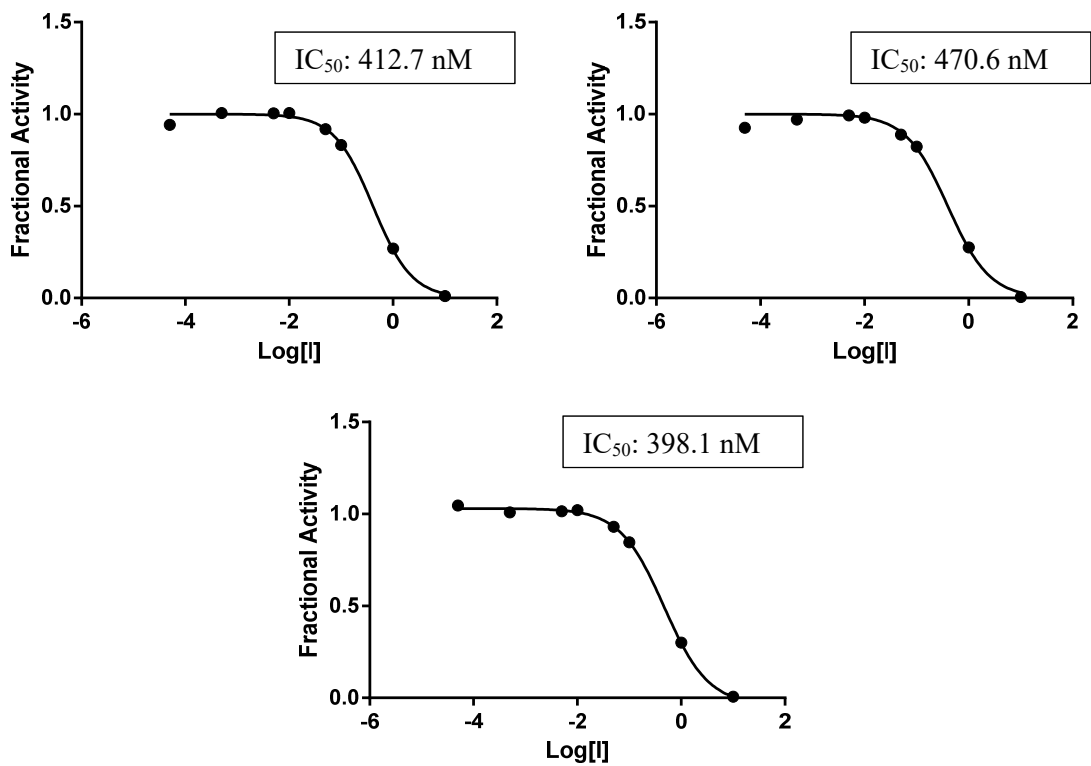


Figure 26: IC_{50} results for KGP382

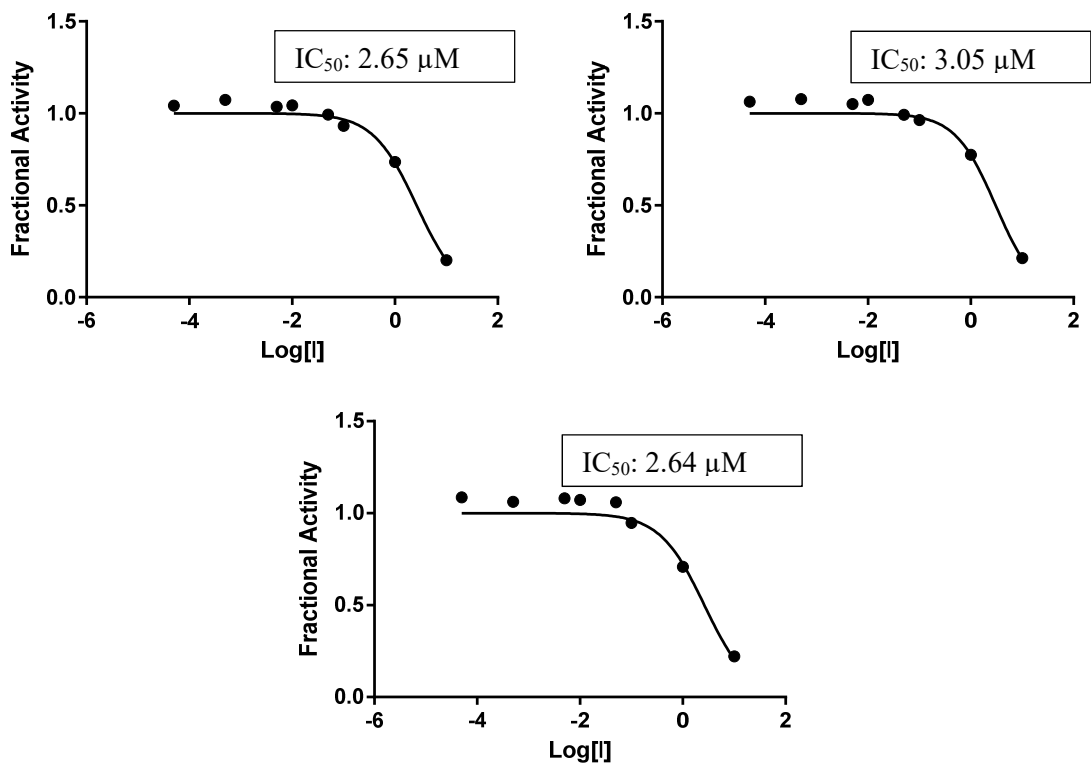


Figure 27: IC_{50} results for KGP384

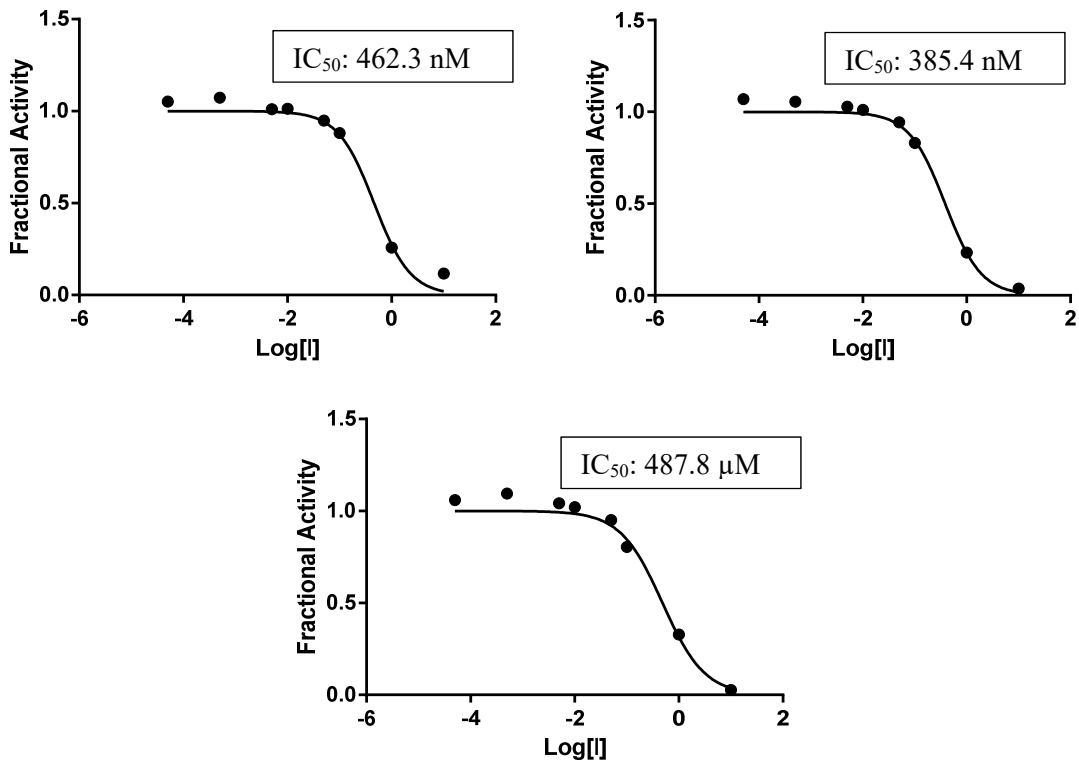


Figure 28: IC_{50} results for KGP385

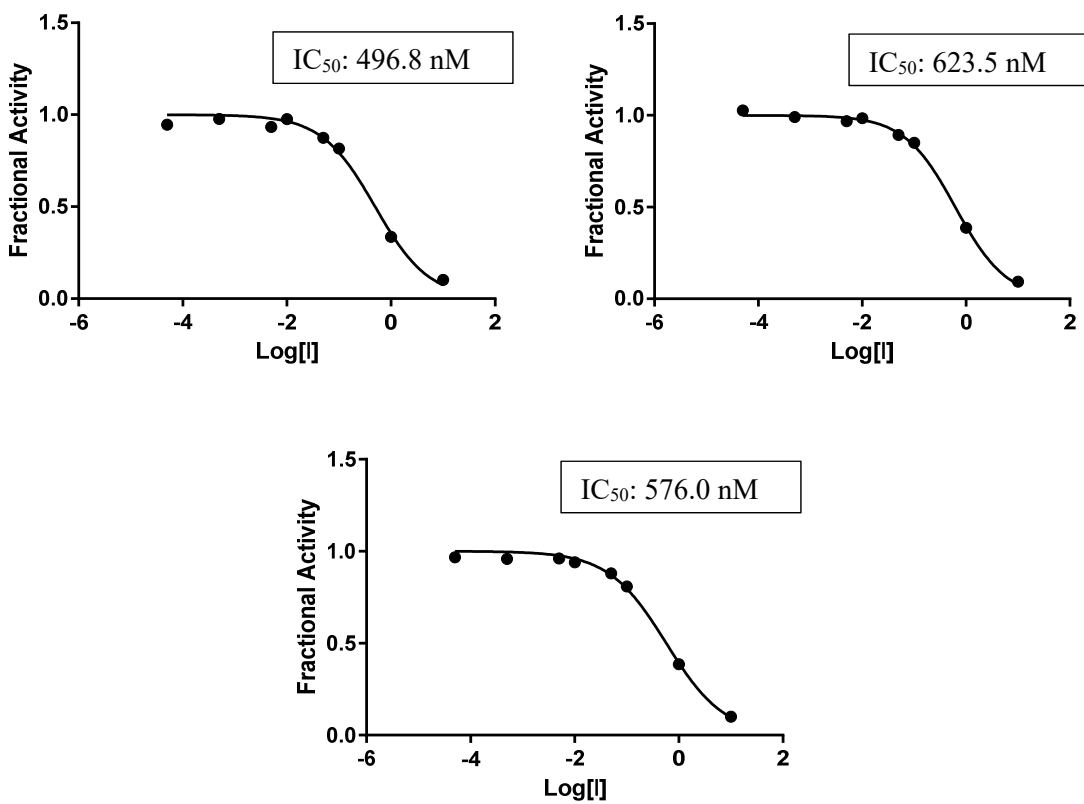


Figure 29: IC_{50} results for KGP388

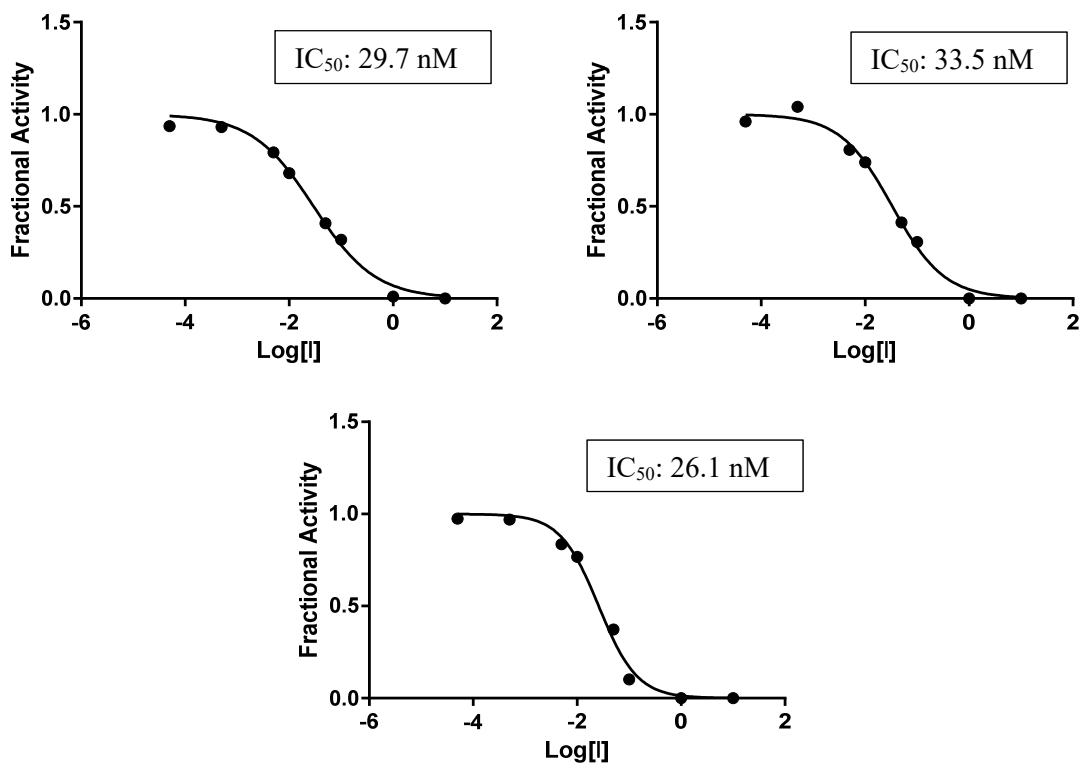


Figure 30: IC_{50} results for KGP402

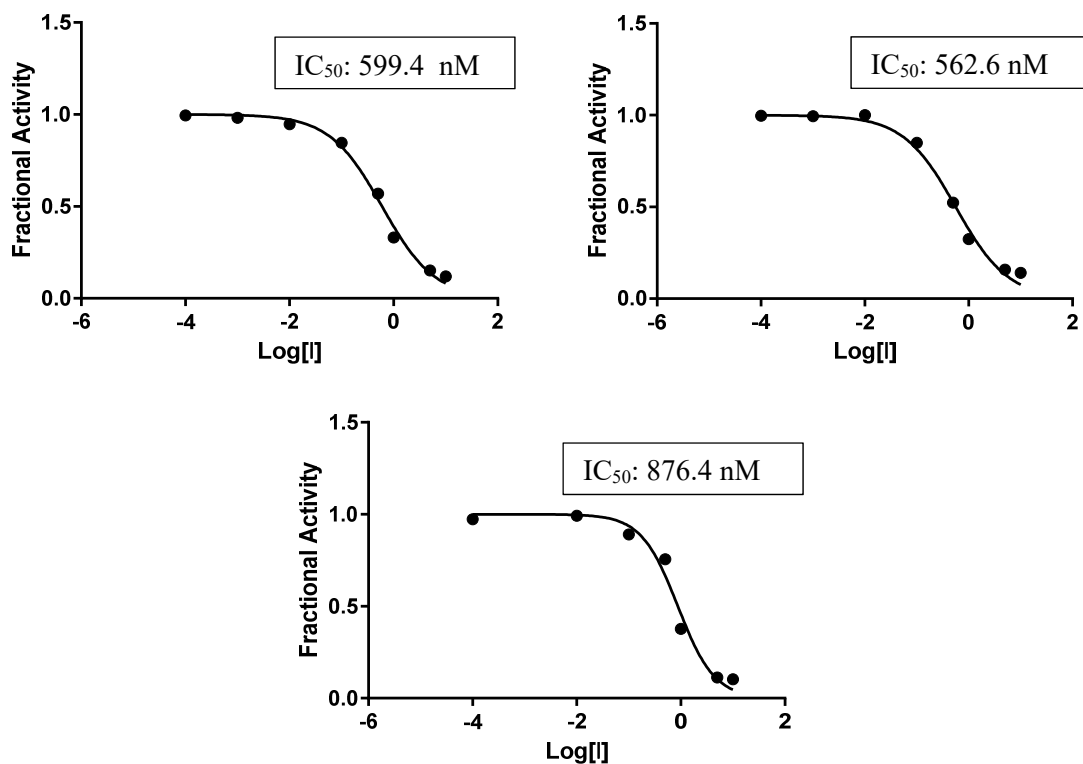


Figure 31: IC_{50} results for KGP406

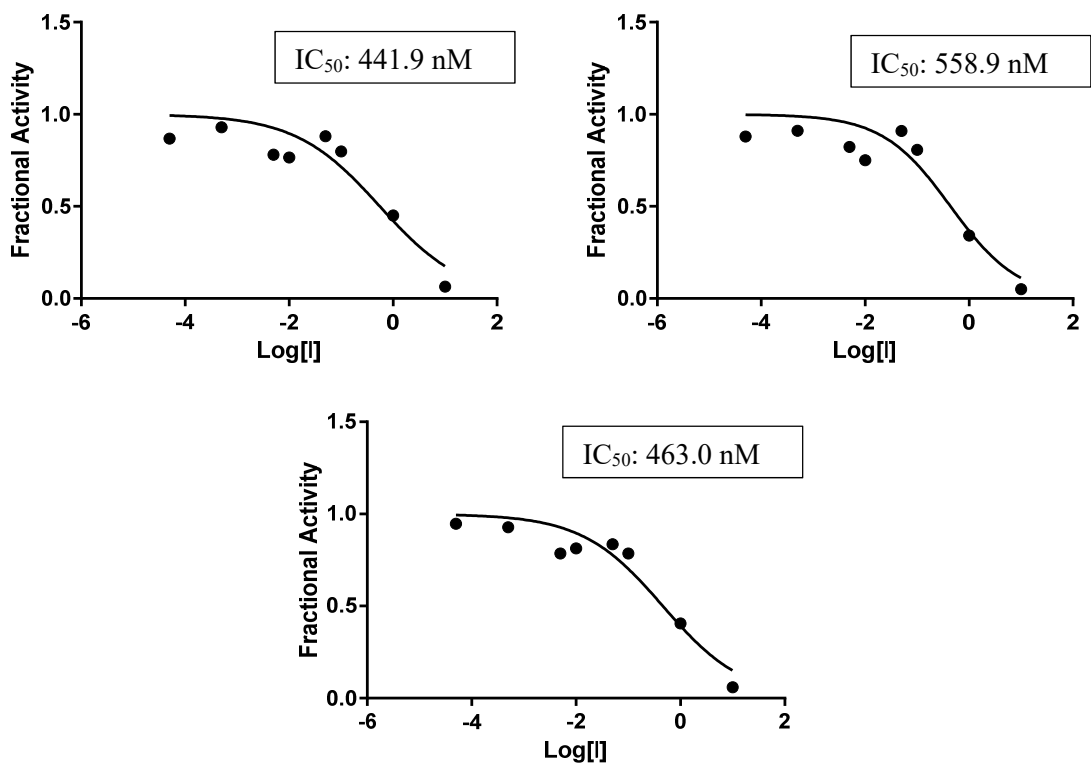


Figure 32: IC_{50} results for KGP421

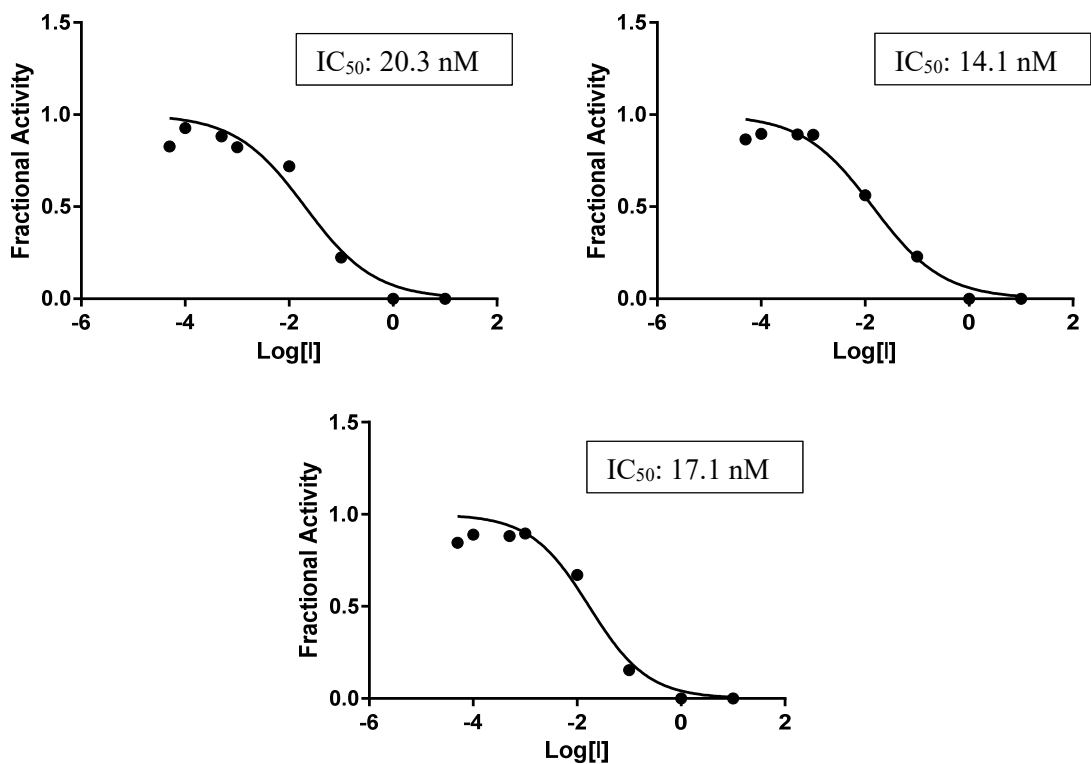


Figure 33: IC_{50} results for KGP434

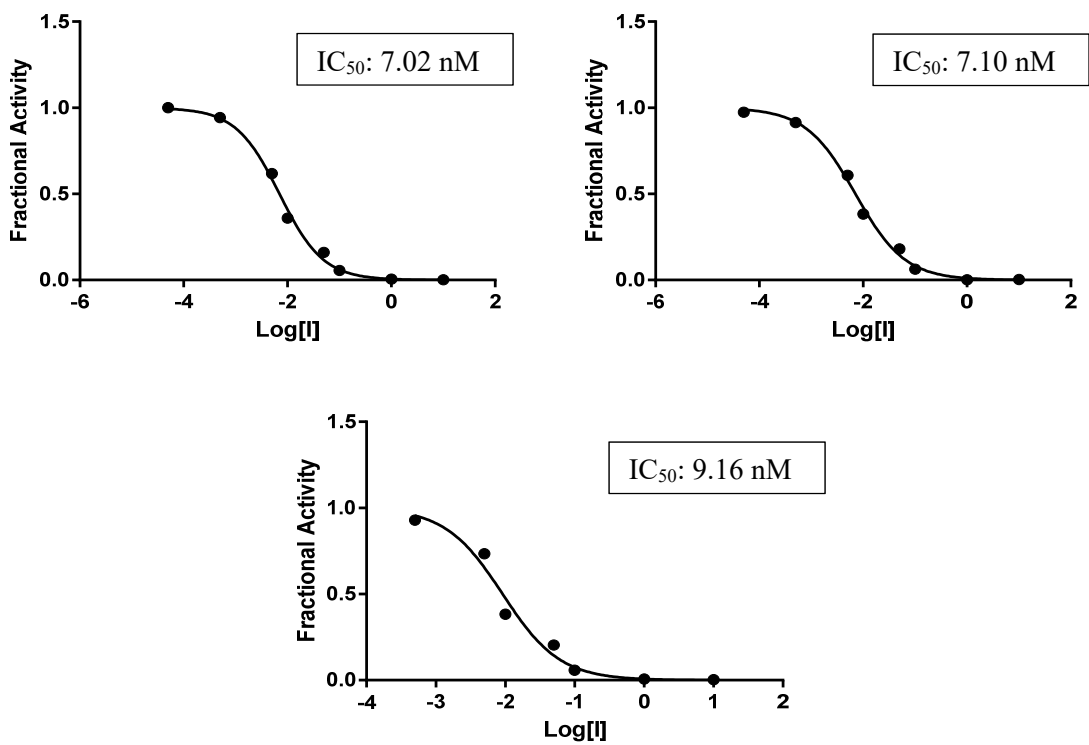


Figure 34: IC_{50} results for KGP434 using 5 μ M substrate

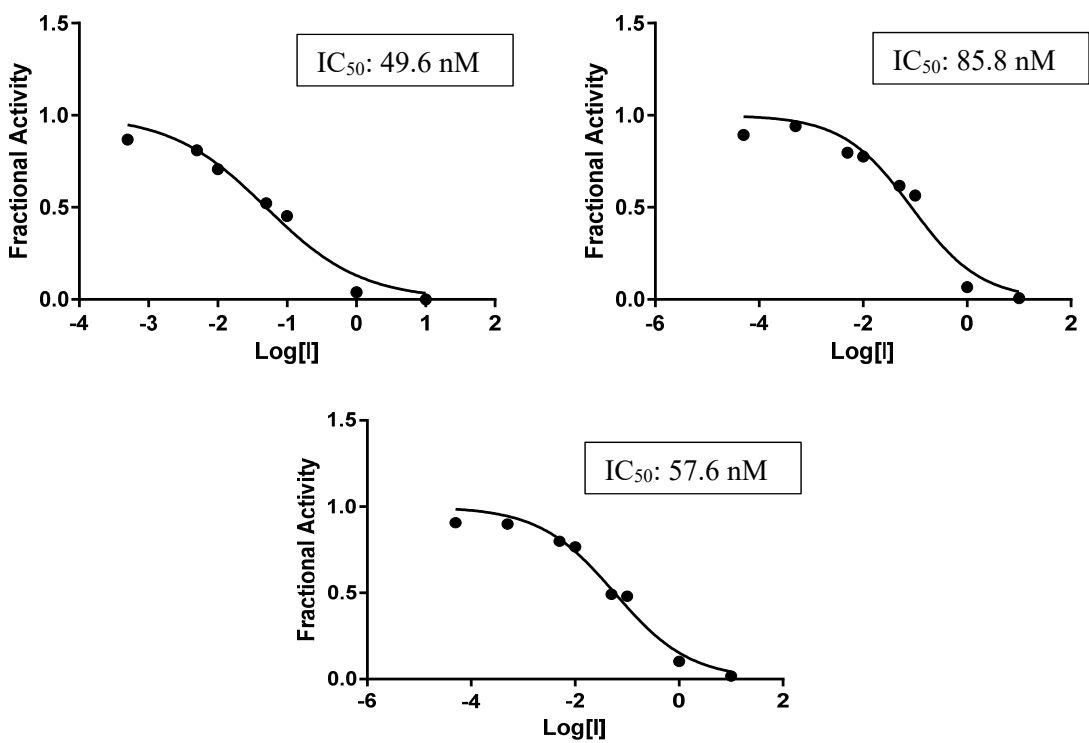


Figure 35: IC_{50} results for KGP435

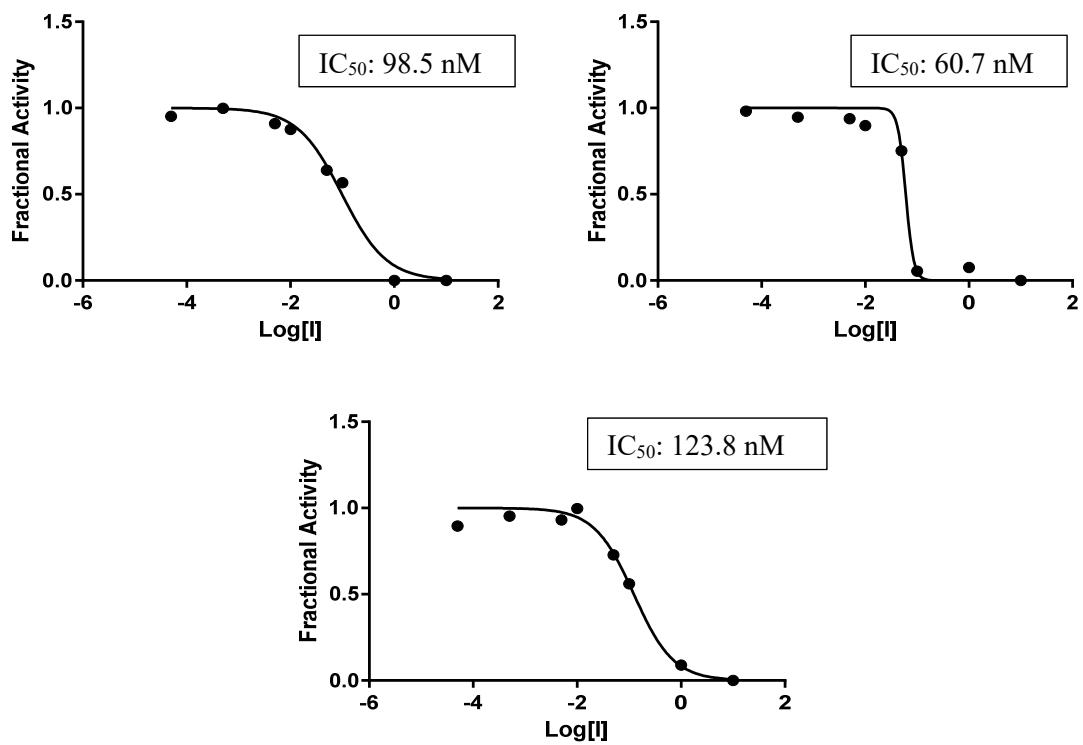


Figure 36: IC_{50} results for KGP451

APPENDIX B

Protocol for Cruzain Inhibitor Reversibility Study

In this assay, cruzain and the inhibitor of interest are incubated at high concentrations to ensure that the enzyme is fully inhibited. This incubation solution is then diluted one hundred-fold. If an inhibitor is reversible, it will disassociate over time and the enzyme activity recovers. If it is irreversible, no disassociation will occur, and the enzyme will not recover any activity. The change in activity over time can be observed using a fluorometer and fluorogenic substrate.

Required Chemicals

- EDTA (40 mM)
- DTT 80 mM
- Sodium Acetate (NaOAc) buffer (pH 5.5, 400mM)
- Substrate (Z-FR-AMC) (6mM)
- Brj-35 (10% by volume)
- Cruzain (1.1 μ M)
- DMSO (100%)

Required Materials and Instruments

- Single channel pipettes (10 μ l, 200 μ l, 1000 μ l,)
- Eight-channel pipette (20-300 μ l)
- Eppendorf Tubes
- 15 mL falcon tubes
- Fluorometer (Fluoroskan Ascent FL)
- 96-Well microplate (black)
- Aluminum foil

Procedure

Incubation

In order to begin incubating the concentrated enzyme and inhibitor solutions, it is necessary to make up an enzyme solution and inhibitor solutions each with one hundred times the normal concentration (100X). The normal enzyme concentration is standard for every cruzain assay (1.1 nM), so the following table can be used to make the 100X enzyme solution. If it is necessary to vary the cruzain concentration, the volume of cruzain can be increased or decreased and the volume of water added should be altered to keep the total volume consistent.

Total Volume	EDTA	DTT	NaOAc	H ₂ O	1:50 Brj	Cruzain
100 μ l	2.5 μ l	3.13 μ l	25 μ l	56.58 μ l	5 μ l	7.8 μ l

Table 1: Formula for 100X enzyme solution

The concentration of inhibitor is more variable since it must be determined according to the potency of the inhibitor being tested. For the reversibility study, two inhibitor solutions should be made with different concentrations. Inhibitor solution 1 should be made so that the inhibitor concentration during incubation is one hundred times the IC₅₀ for that particular inhibitor, and inhibitor solution 2 should be made with an incubation concentration of 5 μ M. The table below gives the formula for the 5 μ M inhibitor solution and a 1.7 μ M solution which can be used as an example for calculating the necessary concentration.

Solution	Concentration in incubation solution	Initial concentration	Stock solution	Volume of stock solution	DMSO	H ₂ O
----------	--------------------------------------	-----------------------	----------------	--------------------------	------	------------------

1	1.7 μ M	34 μ M	200 μ M	17 μ l	18 μ l	65 μ l
2	5 μ M	100 μ M	2 mM	5 μ l	30 μ l	65 μ l

Table 2: Formula for 100X inhibitor solutions

Since the incubation should have similar conditions as the reaction, it is necessary to make a 2.5% DMSO solution (2.5 μ l DMSO + 97.5 μ l H₂O) to substitute for the normal substrate solution. Likewise, the assay buffer should be made according to the following table.

Total Volume	EDTA	DTT	NaOAc	H ₂ O	Brj
1000 μ l	32.5 μ l	40.625 μ l	325 μ l	600.575 μ l	1.3 μ l

Table 3: Formula for the assay buffer

Once enzyme solution, inhibitor solutions, assay buffer, and 2.5% DMSO have been made, the incubation can be started according to the following steps.

- 1) Add 100 μ l of assay buffer to a 1.5 mL Eppendorf tube labeled “1”
- 2) Add 70 μ l of enzyme solution to tube 1
- 3) Add 20 μ l of 2.5 % DMSO solution to tube 1
- 4) Add 10 μ l of inhibitor solution 1 to tube 1
- 5) Repeat steps 1-3 with an Eppendorf tube labeled “2”
- 6) Add 10 μ l of inhibitor solution 2 to tube 2
- 7) Allow both solutions to incubate for ~1 hour

Dilution

While the solutions are incubating, the buffer used to dilute the concentrated solutions (referred to as dilution buffer) should be prepared. This buffer is similar to the standard assay buffer with the addition of the substrate so that the reaction can begin immediately upon dilution. Since this solution contains light sensitive substrate, it should

be covered with foil until it is used. The following table can be used to make the dilution buffer.

Total Volume	EDTA	DTT	H ₂ O	NaOAc	6 mM substrate	Brj
1800 µl	45 µl	56.25 µl	1201.95 µl	450 µl	45 µl	1.8 µl

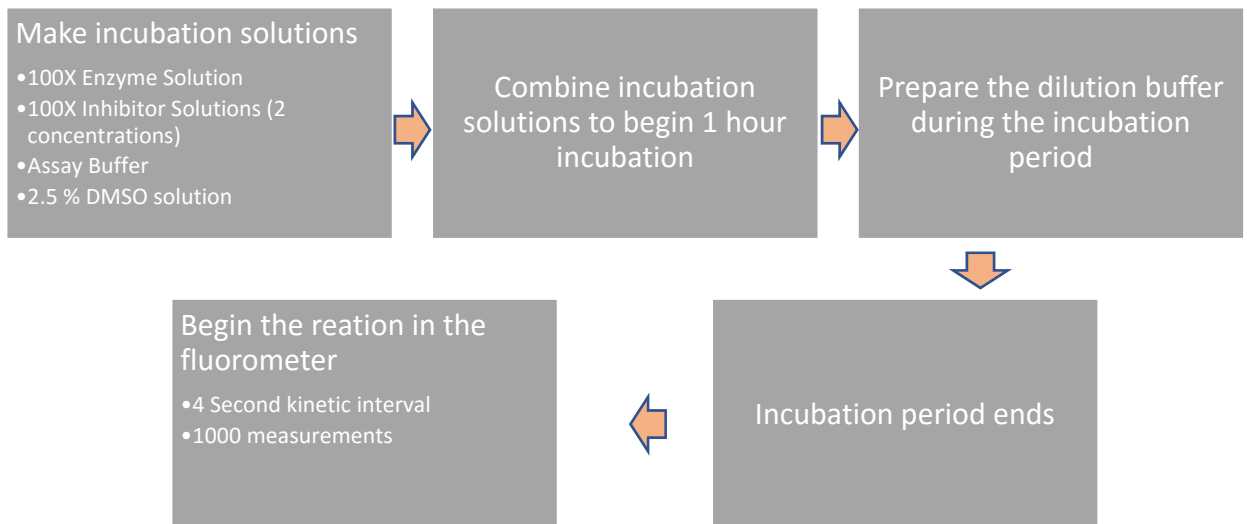
Table 4: Formula for dilution buffer

As soon as the incubation is complete, add 198 µl of the dilution buffer to two wells of a black 96-well plate. Next, add 2 µl of incubation solution 1 to one of the wells, and add 2 µl of incubation solution 2 to the other well.

Measurement

After the incubated solutions have been diluted, the reaction has begun. Immediately place the plate in the fluorescence plate reader and begin measuring the fluorescence at 4 second intervals for 1000 total measurements.

Workflow



Conclusion

Once this protocol has been completed, the data should show whether the enzyme recovers activity over time. The recovery can be quantified by fitting a line to a small portion of the data at the beginning which gives the initial rate of the reaction. Another line fitted to a small portion at the end of the data gives the rate of the reaction at the end of the experiment. If the reaction rate increases significantly, this indicates that the inhibition is reversible. If no change in rate is observed, the inhibition is irreversible.

REFERENCES

- (1) Center for Disease Control. Parasites - American Trypanosomiasis (also known as Chagas Disease) <https://www.cdc.gov/parasites/chagas/index.html> (accessed Feb 12, 2018).
- (2) Curtis-Robles, R.; Auckland, L. D.; Snowden, K. F.; Hamer, G. L.; Hamer, S. A. Analysis of over 1500 Triatomine Vectors from across the US, Predominantly Texas, for *Trypanosoma Cruzi* Infection and Discrete Typing Units. *Infect. Genet. Evol.* **2018**, *58*, 171–180.
- (3) PAHO WHO | Chagas disease
http://www.paho.org/hq/index.php?option=com_topics&view=article&id=10&Itemid=40743&lang=en (accessed Feb 12, 2018).
- (4) GBD 2015 Disease and Injury Incidence and Prevalence Collaborators. Global, Regional, and National Incidence, Prevalence, and Years Lived with Disability for 310 Diseases and Injuries, 1990–2015: A Systematic Analysis for the Global Burden of Disease Study 2015. *Lancet Lond. Engl.* **2016**, *388* (10053), 1545–1602.
- (5) Hotez, P. J.; Alvarado, M.; Basáñez, M.-G.; Bolliger, I.; Bourne, R.; Boussinesq, M.; Brooker, S. J.; Brown, A. S.; Buckle, G.; Budke, C. M.; et al. The Global Burden of Disease Study 2010: Interpretation and Implications for the Neglected Tropical Diseases. *PLoS Negl. Trop. Dis.* **2014**, *8* (7), e2865.
- (6) Kjos, S. A.; Snowden, K. F.; Craig, T. M.; Lewis, B.; Ronald, N.; Olson, J. K. Distribution and Characterization of Canine Chagas Disease in Texas. *Vet. Parasitol.* **2008**, *152* (3), 249–256.
- (7) Rassi, A.; Marin-Neto, J. A. Chagas Disease. *Lancet Lond.* **2010**, *375* (9723), 1388–1402.
- (8) Tyler, K. M.; Olson, C. L.; Engman, D. M. The Life Cycle Of *Trypanosoma Cruzi*. In *American Trypanosomiasis*; World Class Parasites; Springer, Boston, MA, 2003; pp 1–11.
- (9) Brener, Z. Biology of *Trypanosoma Cruzi*. *Annu. Rev. Microbiol.* **1973**, *27* (1), 347–382.
- (10) CDC. CDC - Chagas Disease - Biology
<http://www.cdc.gov/parasites/chagas/biology.html> (accessed Mar 4, 2018).
- (11) Schofield, C. J.; Galvão, C. Classification, Evolution, and Species Groups within the Triatominae. *Acta Trop.* **2009**, *110* (2), 88–100.

- (12) Klotz, S. A.; Dorn, P. L.; Mosbacher, M.; Schmidt, J. O. Kissing Bugs in the United States: Risk for Vector-Borne Disease in Humans. *Environ. Health Insights* **2014**, 8s2, EHI.S16003.
- (13) Texas A&M Veterinary & Biomedical. Kissing Bugs and Chagas Disease in the U.S. | Texas A&M University <http://kissingbug.tamu.edu> (accessed Mar 6, 2018).
- (14) Cesa, K.; Caillouët, K. A.; Dorn, P. L.; Wesson, D. M. High *Trypanosoma Cruzi* (Kinetoplastida: Trypanosomatidae) Prevalence in *Triatoma Sanguisuga* (Hemiptera: Reduviidae) in Southeastern Louisiana. *J. Med. Entomol.* **2011**, 48 (5), 1091–1094.
- (15) Dorn, P. L.; Perniciaro, L.; Yabsley, M. J.; Roellig, D. M.; Balsamo, G.; Diaz, J.; Wesson, D. Autochthonous Transmission of *Trypanosoma Cruzi*, Louisiana. *Emerg. Infect. Dis.* **2007**, 13 (4), 605–607.
- (16) Shen, L.; Ramires, F.; Martinez, F.; Bodanese, L. C.; Echeverría, L. E.; Gómez, E. A.; Abraham, W. T.; Dickstein, K.; Køber, L.; Packer, M.; et al. Contemporary Characteristics and Outcomes in Chagasic Heart Failure Compared With Other Nonischemic and Ischemic Cardiomyopathy. *Circ. Heart Fail.* **2017**, 10 (11).
- (17) Matsuda, N. M.; Miller, S. M.; Evora, P. R. B. The Chronic Gastrointestinal Manifestations of Chagas Disease. *Clinics* **2009**, 64 (12), 1219–1224.
- (18) Beaumier, C. M.; Gillespie, P. M.; Strych, U.; Hayward, T.; Hotez, P. J.; Bottazzi, M. E. Status of Vaccine Research and Development of Vaccines for Chagas Disease. *Vaccine* **2016**, 34 (26), 2996–3000.
- (19) Longo, D. L.; Bern, C. Chagas' Disease. *N. Engl. J. Med. Boston* **2015**, 373 (5), 456–466.
- (20) Viotti, R.; Vigliano, C.; Lococo, B.; Bertocchi, G.; Petti, M.; Alvarez, M. G.; Postan, M.; Armenti, A. Long-Term Cardiac Outcomes of Treating Chronic Chagas Disease with Benznidazole versus No Treatment: A Nonrandomized Trial. *Ann. Intern. Med.* **2006**, 144 (10), 724–734.
- (21) Aldasoro, E.; Posada, E.; Requena-Méndez, A.; Calvo-Cano, A.; Serret, N.; Casellas, A.; Sanz, S.; Soy, D.; Pinazo, M. J.; Gascon, J. What to Expect and When: Benznidazole Toxicity in Chronic Chagas' Disease Treatment. *J. Antimicrob. Chemother.* **2018**.
- (22) Commissioner, O. of the. Press Announcements - FDA approves first U.S. treatment for Chagas disease <https://www.fda.gov/NewsEvents/Newsroom/PressAnnouncements/ucm573942.htm> (accessed Feb 12, 2018).

- (23) Manne-Goehler, J.; Umeh, C. A.; Montgomery, S. P.; Wirtz, V. J. Estimating the Burden of Chagas Disease in the United States. *PLoS Negl. Trop. Dis.* **2016**, *10* (11), e0005033.
- (24) Cantey Paul T.; Stramer Susan L.; Townsend Rebecca L.; Kamel Hany; Ofafa Karen; Todd Charles W.; Currier Mary; Hand Sheryl; Varnado Wendy; Dotson Ellen; et al. The United States Trypanosoma Cruzi Infection Study: Evidence for Vector-borne Transmission of the Parasite That Causes Chagas Disease among United States Blood Donors. *Transfusion (Paris)* **2012**, *52* (9), 1922–1930.
- (25) Garcia, M. N.; Aguilar, D.; Gorchakov, R.; Rossmann, S. N.; Montgomery, S. P.; Rivera, H.; Woc-Colburn, L.; Hotez, P. J.; Murray, K. O. Evidence of Autochthonous Chagas Disease in Southeastern Texas. *Am. J. Trop. Med. Hyg.* **2015**, *92* (2), 325–330.
- (26) Gunter, S. M.; Murray, K. O.; Gorchakov, R.; Beddard, R.; Rossmann, S. N.; Montgomery, S. P.; Rivera, H.; Brown, E. L.; Aguilar, D.; Widman, L. E.; et al. Likely Autochthonous Transmission of Trypanosoma Cruzi to Humans, South Central Texas, USA. *Emerg. Infect. Dis.* **2017**, *23* (3), 500–503.
- (27) Estrada-Franco, J. G.; Bhatia, V.; Diaz-Albiter, H.; Ochoa-Garcia, L.; Barbabosa, A.; Vazquez-Chagoyan, J. C.; Martinez-Perez, M. A.; Guzman-Bracho, C.; Garg, N. Human Trypanosoma Cruzi Infection and Seropositivity in Dogs, Mexico. *Emerg. Infect. Dis.* **2006**, *12* (4), 624–630.
- (28) Guzman-Tapia, Y.; Ramirez-Sierra, M. J.; Escobedo-Ortegon, J.; Dumonteil, E. Effect of Hurricane Isidore on Triatoma Dimidiata Distribution and Chagas Disease Transmission Risk in the Yucatán Peninsula of Mexico. *Am. J. Trop. Med. Hyg.* **2005**, *73* (6), 1019–1025.
- (29) Vidal, J. C.; Alcantara, C. D. L.; De Souza, W.; Cunha-E-Silva, N. L. Lysosome-like Compartments of Trypanosoma Cruzi Trypomastigotes May Originate Directly from Epimastigote Reservosomes. *Parasitol. Camb.* **2017**, *144* (6), 841–850.
- (30) Klemba, M.; Goldberg, and D. E. Biological Roles of Proteases in Parasitic Protozoa. *Annu. Rev. Biochem.* **2002**, *71* (1), 275–305.
- (31) Andrade, D.; Serra, R.; Svensjö, E.; Lima, A. P. C.; Ramos Junior, E. S.; Fortes, F. S.; Morandini, A. C. F.; Morandi, V.; Soeiro, M. de N.; Tanowitz, H. B.; et al. Trypanosoma Cruzi Invades Host Cells through the Activation of Endothelin and Bradykinin Receptors: A Converging Pathway Leading to Chagasic Vasculopathy. *Br. J. Pharmacol.* **2012**, *165* (5), 1333–1347.
- (32) Aparicio, I. M.; Scharfstein, J.; Lima, A. P. C. A. A New Cruzipain-Mediated Pathway of Human Cell Invasion by Trypanosoma Cruzi Requires Trypomastigote Membranes. *Infect. Immun.* **2004**, *72* (10), 5892–5902.

- (33) Doyle, P. S.; Zhou, Y. M.; Hsieh, I.; Greenbaum, D. C.; McKerrow, J. H.; Engel, J. C. The Trypanosoma Cruzi Protease Cruzain Mediates Immune Evasion. *PLoS Pathog.* **2011**, 7 (9), e1002139.
- (34) Avelar, L. A. A.; Camilo, C. D.; Albuquerque, S. de; Fernandes, W. B.; Gonzalez, C.; Kenny, P. W.; Leitão, A.; McKerrow, J. H.; Montanari, C. A.; Orozco, E. V. M.; et al. Molecular Design, Synthesis and Trypanocidal Activity of Dipeptidyl Nitriles as Cruzain Inhibitors. *PLoS Negl. Trop. Dis.* **2015**, 9 (7), e0003916.
- (35) Engel, J. C.; Torres, C.; Hsieh, I.; Doyle, P. S.; McKerrow, J. H.; Garcia, C. T. Upregulation of the Secretory Pathway in Cysteine Protease Inhibitor-Resistant Trypanosoma Cruzi. *J. Cell Sci.* **2000**, 113 (Pt 8), 1345–1354.
- (36) Engel, J. C.; Doyle, P. S.; Hsieh, I.; McKerrow, J. H. Cysteine Protease Inhibitors Cure an Experimental Trypanosoma Cruzi Infection. *J. Exp. Med.* **1998**, 188 (4), 725–734.
- (37) Huang, L.; Brinen, L. S.; Ellman, J. A. Crystal Structures of Reversible Ketone-Based Inhibitors of the Cysteine Protease Cruzain. *Bioorg. Med. Chem.* **2003**, 11 (1), 21–29.
- (38) Eakin, A. E.; Mills, A. A.; Harth, G.; McKerrow, J. H.; Craik, C. S. The Sequence, Organization, and Expression of the Major Cysteine Protease (Cruzain) from Trypanosoma Cruzi. *J. Biol. Chem.* **1992**, 267 (11), 7411–7420.
- (39) Zhai, X.; Meek, T. D. Catalytic Mechanism of Cruzain from Trypanosoma Cruzi As Determined from Solvent Kinetic Isotope Effects of Steady-State and Pre-Steady-State Kinetics. *Biochemistry (Mosc.)* **2018**.
- (40) Parker, E. N. Design and Synthesis of Small-Molecule Inhibitors of Cathepsin L Bearing the Thiosemicarbazone Warhead as Potential Anti-Metastatic Agents. Thesis, 2015.
- (41) Siles, R.; Chen, S.-E.; Zhou, M.; Pinney, K. G.; Trawick, M. L. Design, Synthesis, and Biochemical Evaluation of Novel Cruzain Inhibitors with Potential Application in the Treatment of Chagas' Disease. *Bioorg. Med. Chem. Lett.* **2006**, 16 (16), 4405–4409.
- (42) Kumar, G. D. K.; Chavarria, G. E.; Charlton-Sevcik, A. K.; Yoo, G. K.; Song, J.; Strecker, T. E.; Siim, B. G.; Chaplin, D. J.; Trawick, M. L.; Pinney, K. G. Functionalized Benzophenone, Thiophene, Pyridine, and Fluorene Thiosemicarbazone Derivatives as Inhibitors of Cathepsin L. *Bioorg. Med. Chem. Lett.* **2010**, 20 (22), 6610–6615.
- (43) Kishore Kumar, G. D.; Chavarria, G. E.; Charlton-Sevcik, A. K.; Arispe, W. M.; Macdonough, M. T.; Strecker, T. E.; Chen, S.-E.; Siim, B. G.; Chaplin, D. J.; Trawick, M. L.; et al. Design, Synthesis, and Biological Evaluation of Potent

Thiosemicarbazone Based Cathepsin L Inhibitors. *Bioorg. Med. Chem. Lett.* **2010**, 20 (4), 1415–1419.

- (44) Parker, E. N.; Song, J.; Kishore Kumar, G. D.; Odutola, S. O.; Chavarria, G. E.; Charlton-Sevcik, A. K.; Strecker, T. E.; Barnes, A. L.; Sudhan, D. R.; Wittenborn, T. R.; et al. Synthesis and Biochemical Evaluation of Benzoylbenzophenone Thiosemicarbazone Analogues as Potent and Selective Inhibitors of Cathepsin L. *Bioorg. Med. Chem.* **2015**, 23 (21), 6974–6992.
- (45) Parker, E. N.; Odutola, S. O.; Wang, Y.; Strecker, T. E.; Mukherjee, R.; Shi, Z.; Chaplin, D. J.; Trawick, M. L.; Pinney, K. G. Synthesis and Biological Evaluation of a Water-Soluble Phosphate Prodrug Salt and Structural Analogues of KGP94, a Lead Inhibitor of Cathepsin L. *Bioorg. Med. Chem. Lett.* **2017**, 27 (5), 1304–1310.
- (46) Strelow, J.; Dewe, W.; Iversen, P. W.; Brooks, H. B.; Radding, J. A.; McGee, J.; Weidner, J. Mechanism of Action Assays for Enzymes. In *Assay Guidance Manual*; Sittampalam, G. S., Coussens, N. P., Brimacombe, K., Grossman, A., Arkin, M., Auld, D., Austin, C., Baell, J., Bejcek, B., Chung, T. D. Y., et al., Eds.; Eli Lilly & Company and the National Center for Advancing Translational Sciences: Bethesda (MD), 2004.